Joint Impacts of Intraseasonal Oscillation and Diurnal Cycle on East Asian Summer Monsoon Rainfall

BIQI LIU,[a,b] GUIXING CHEN,[a] AND HUILING QIN[a]

[a] *Southern Marine Science and Engineering Guangdong Laboratory (Zhuhai), and School of Atmospheric Sciences, Sun Yat-sen University, Zhuhai, China*
[b] *Dongguan Meteorological Bureau, Dongguan, China*

(Manuscript received 12 May 2023, in final form 7 October 2023, accepted 11 October 2023)

ABSTRACT: Intraseasonal and diurnal variations are two basic periodic oscillations in global/regional climate and weather. To investigate their joint impacts over East Asia, this paper categorizes the boreal summer intraseasonal oscillations (ISOs) in 1998–2019 into two groups with different diurnal cycles. It is shown that the active ISOs with large diurnal cycles feature a northwestward-moving anomalous anticyclone with strong southerlies at the western flank. These ISOs have in-phase patterns of geopotential height anomaly between low and midlatitudes over East Asia, associated with the simultaneous expansions of the western Pacific subtropical high (WPSH) and South Asian high (SAH). They couple with the anomalous ABL heating by daytime solar radiation over East Asia, which acts to enhance monsoon southerlies at midnight. The nocturnally strengthened southerlies facilitate dynamic lifting, moisture transport, and convective instability for producing midnight to morning rainfall at their northern terminus, thereby yielding a remarkable northward propagation of the monsoon rain belt. In contrast, the other ISOs with small diurnal cycles are related to a westward-moving anomalous anticyclone, while the WPSH and SAH have relatively small expansions and the westerly trough is active at middle latitudes. They lead to the dipole patterns of geopotential height anomaly and weak ABL heating over East Asia. The daily-mean southerlies and moisture conditions as well as their nocturnal enhancements are relatively weak, and thus, the northward shift of the monsoon rain belt is less pronounced. These results highlight that the large-scale conditions of ISOs can be distinguished by their different couplings with regional-scale diurnal forcings, which help the understanding and prediction of multiscale rainfall activities.

KEYWORDS: Monsoons; Precipitation; Rainfall; Summer/warm season; Diurnal effects; Intraseasonal variability

1. Introduction

The East Asian summer monsoon (EASM) exhibits evident variabilities from diurnal to interdecadal time scales (Chen et al. 2004; Ding and Chan 2005; Chang et al. 2018). The active monsoon southerlies march northward in a stepwise manner from southern China to central China and southern Japan in mid-June, and to northern China, the Korean Peninsula, and northern Japan in mid-July, in association with the propagation of intraseasonal oscillations (ISOs) (Qian et al. 2002; Wang and LinHo 2002; Ding and Chan 2005). The active EASM is also characterized by the synoptic-scale monsoon surges of strong southerlies lasting for days or weeks (Zhang et al. 2002; Y. Ding et al. 2021; Liu et al. 2022). The monsoonal fluctuations at both intraseasonal and synoptic time scales are important to the repeated occurrences of heavy rain over East Asia (Liu et al. 2014; Li and Zhou 2015; L. Ding et al. 2021; Y. Ding et al. 2021). At shorter time scales, monsoon southerlies tend to show diurnal variations with a maximum at midnight, helping to produce MCSs and torrential rainfall in the following morning (Chen et al. 2009; G. Chen et al. 2017; Sun and Zhang 2012; Shin et al. 2019; Guan et al. 2020). These monsoon activities from diurnal to intraseasonal time scales are linked with the interannual and interdecadal variations of the EASM rain belt (Ding and Chan 2005; Chen 2020; Chen et al. 2021). Further studies on the multiscale interactions of EASM are needed for seamless prediction across time scales and for the prevention of meteorological disasters (Ren et al. 2023).

The 10–90-day ISO in the summertime, mainly propagating from tropical oceans to extratropical East Asia, is thought to be an important signal in the gap between weather forecast and climate prediction (Li and Wang 2005; Cao et al. 2017; H. Wang et al. 2021). The active phases of ISOs feature low-level cyclonic vorticity and moisture transport in association with frequent southerly monsoon surges (Yang and Li 2003; Hsu et al. 2016; Y. Ding et al. 2021). Thus, the active phases provide favorable background conditions for the development of synoptic disturbances and tropical cyclones, producing continuous wet episodes (Hsu et al. 2016; Ling et al. 2016; Liu et al. 2022). In contrast, the suppressed phases of ISOs tend to coexist with dry episodes and/or heat waves (Hsu et al. 2017; Chen et al. 2018; Gao et al. 2018). The ISOs have an inherent property with tropical and extratropical large-scale interactions, which affect the weather and climate from tropical to midlatitude regions (Ko and Hsu 2006; Fujinami and Yasunari 2009; Yang et al. 2014). Moreover, ISOs can have diverse impacts over East Asia through various land surface processes.

Supplemental information related to this paper is available at the Journals Online website: https://doi.org/10.1175/JCLI-D-23-0284.s1.

Corresponding authors: Guixing Chen, chenguixing@mail.sysu.edu.cn; Huiling Qin, qinhling@mail.sysu.edu.cn

DOI: 10.1175/JCLI-D-23-0284.1

They may couple with elevated terrains or daytime insolation (Chen and Takahashi 1995; Natoli and Maloney 2019; Chudler et al. 2020), in which high-frequency regional dynamic or thermodynamic forcings may join to regulate the weather systems. However, the coupling of intraseasonal large-scale oscillations and high-frequency regional forcings during the EASM seasons has not been convincingly explained yet.

The diurnal cycle is another basic fluctuation in the atmosphere (Moncrieff et al. 2007), which is pronounced over the heated continent in summer (Krishnamurti and Kishtawal 2000; Chow and Chan 2009; Chen 2020). In the Asian monsoon regions, diurnal cycles of low-level winds exhibit a maximum wind speed at midnight (Chen et al. 2009; Yu et al. 2009; Wang et al. 2013). Large diurnal amplitudes tend to occur with strong background monsoon southwesterlies, which is referred to as diurnal monsoon variability (DMV) (Chen et al. 2009; Xue et al. 2018; Chen 2020). The wind diurnal cycle is expressed as a regional-scale dynamic response to daytime heating that induces vertical turbulent mixing in the boundary layer (Blackadar 1957) or horizontal thermal contrast along sloping terrains (Holton 1967). Over East Asia, the southwesterlies with large DMV are favorable for the formation of nocturnal LLJs that transport warm moist air northward and establish a convective environment at their northern terminus (Chen et al. 2013; Fu et al. 2019; Zhang et al. 2019). Therefore, successive MCSs and extremely heavy rainfall are produced in the following morning (Sun and Zhang 2012; Zhang et al. 2018; Guan et al. 2020). Coupling regional-scale diurnal cycles with large-scale circulations is crucial for climate change. For instance, the DMV coupled with the different expansions of the western Pacific subtropical high (WPSH) has been shown to coincide with the long-term variations of anomalously dry/wet patterns at the intraseasonal, interannual, and interdecadal scales (Chen et al. 2021). The interaction of the DMV and other oscillations at longer time scales is a key scientific issue for the intersection of weather and climate in monsoon regions.

The relationship between intraseasonal variabilities and diurnal cycles of atmospheric signals has received considerable attention in recent years. Fujinami et al. (2017) found that the diurnal cycles of summer rainfall over the southern slopes of the Meghalaya Plateau are more significant in the ISO westerly regimes than in easterly regimes. Chen et al. (2019) showed that the boreal summer intraseasonal oscillation (BSISO) modulates the diurnal cycles of coastal rainfall over south China by large-scale moisture advection and local land–sea breeze circulation. Natoli and Maloney (2019) also examined a similar modulation in the Philippines. Chudler et al. (2020) and Xu et al. (2021) further demonstrated that the diurnal variations of MCS over the South China Sea region vary with large-scale environments, which are influenced by the BSISO activities. Most previous studies focused on how the ISOs modulate the diurnal processes in the tropics with less attention to their interactions in the extratropics. Over East Asia, the monsoon flows are regulated not only by the combined influence of external large-scale forcings from the tropics and midlatitudes (Ninomiya and Shibagaki 2007; Fujinami and Yasunari 2009; Yang et al. 2014; Y. Ding 2021) but also by the pronounced regional-scale forcings due to inhomogeneous topography and land–sea contrasts (Yu et al. 2009; Pan and Chen 2019). Therefore, the joint impacts of intraseasonal and diurnal oscillations during the EASM seasons can be complicated. Although their importance has been proved in some case studies, such as the intense mei-yu–baiu rainfall seasons over East Asia in 1998 and 2020 (Sun et al. 2016; G. Chen et al. 2017; Y. Ding et al. 2021; Zeng et al. 2022), our knowledge of the associated mechanism is still lacking.

The present study aims to analyze the joint impacts of ISOs and DMVs on summer rainfall over East Asia by comparing the ISOs with different DMV amplitudes. The rest of this paper is organized as follows. Section 2 introduces the data and methods used in this study. Section 3 shows the multiscale activities of EASM with particular attention to the ISOs with different DMV amplitudes. Section 4 compares large-scale circulations and regional forcings with different combinations of ISOs and DMVs. Section 5 examines the physical processes that produce rainfall patterns under the combined effects of ISOs and DMVs. Section 6 gives the conclusions and discussion.

2. Data and method

a. *Datasets used in the study*

The atmospheric variables are obtained from the Japanese 55-year Reanalysis (JRA-55) on a 1.25° × 1.25° latitude–longitude grid with a 6-hourly temporal resolution (Kobayashi et al. 2015). JRA-55 gives a good performance in capturing lower-tropospheric conditions with a 25-hPa vertical interval below 750 hPa. Compared with other reanalysis data, it presents better in reproducing the diurnal variations of winds, temperature, and humidity over East Asia (Chen et al. 2014, 2021). JRA-55 has been widely used to study the summertime large-scale circulations and regional forcings over East Asia (e.g., Kudo et al. 2014; He and Liu 2016; Tamaki et al. 2018).

The precipitation data are derived from the Tropical Rainfall Measuring Mission (TRMM 3B42v7). TRMM offers 3-hourly rain rates on a 0.25° × 0.25° grid with calibrations by various satellite systems and rain gauge measurements (Huffman et al. 2007). It has a good quality in performing the diurnal variations of warm-season rainfall over East Asia (Zhou et al. 2008; Koo et al. 2009; Shen et al. 2010). It is also capable of performing the spatial distribution and seasonal evolution of the EASM rain belt (Koo et al. 2009; Xu et al. 2009; Zhao and Yatagai 2014).

The focus of this study is on the summer (June–August) in the past 22 years (1998–2019). Considering that the inertial oscillation of winds induced by daytime solar heating can last until the following morning (Xue et al. 2018; Chen 2020), the diurnal cycle is estimated from 1200 to 1100 LST the next day (LST = UTC + 8 h). The four synoptic hours, 1400, 2000, 0200, and 0800 LST, denote afternoon, evening, midnight, and morning, respectively. The diurnal deviations of any variables are calculated by subtracting the daily mean on the given day.

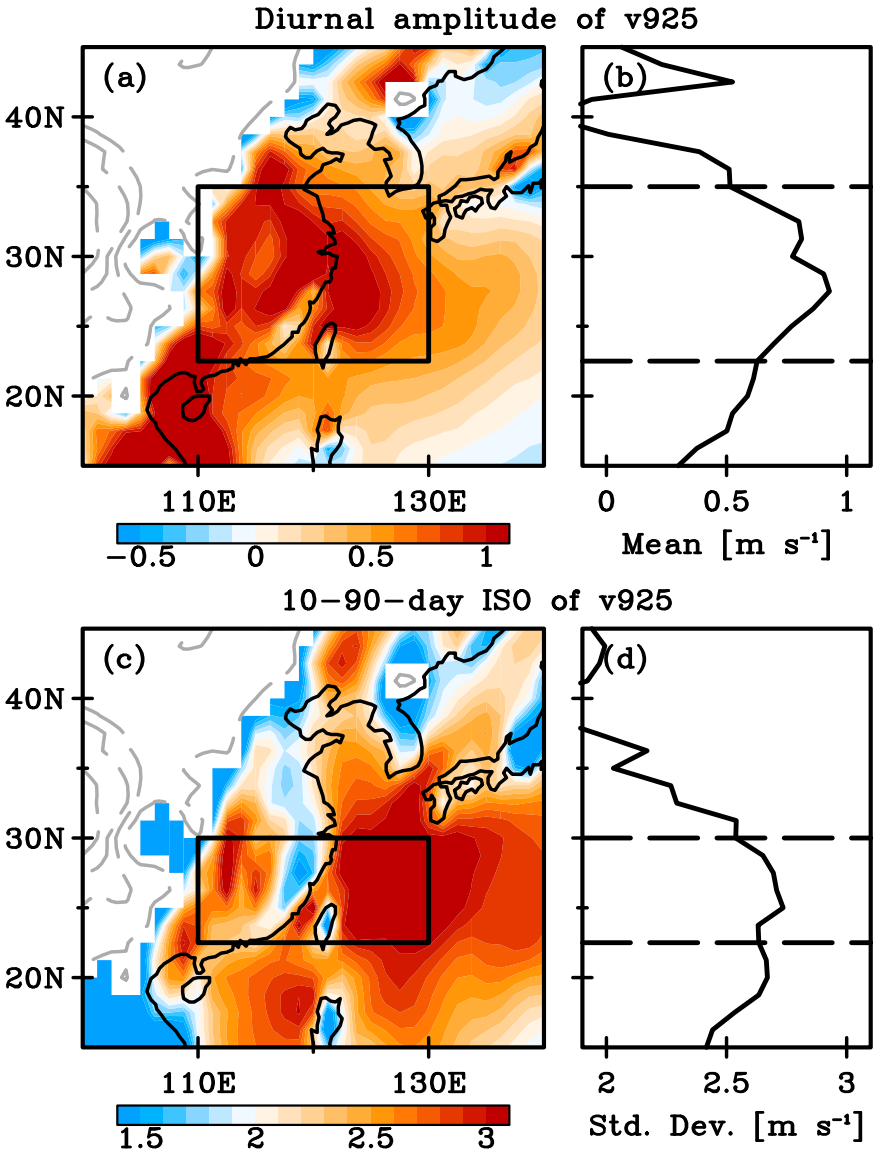

FIG. 1. (a) Climatological mean of the diurnal amplitudes of 925-hPa meridional winds (shading; m s^{-1}) in the summers of 1998–2019. The gray dashed lines denote the elevations with an interval of 1000 m. The box (110°–130°E, 22.5°–35°N) denotes the southern region of subtropical East Asia. (b) Climatological mean of the diurnal amplitudes averaged at 110°–130°E. (c) Standard deviation of the 10–90-day ISOs of 925-hPa meridional winds (shading; m s^{-1}) in the summers of 1998–2019. The box (110°–130°E, 22.5°–30°N) denotes the area to estimate the ISO index. (d) Standard deviation of the 10–90-day ISOs averaged at 110°–130°E.

b. *Definitions of monsoon variabilities at diurnal and intraseasonal time scales*

The monsoon southerlies are represented by the meridional winds at 925 hPa that are greatly affected by diurnally varying ABL processes (Chen 2020). At the diurnal time scale (Figs. 1a,b), the DMV amplitude is measured by the diurnal deviation of meridional winds at 0200 LST when the monsoon southerlies usually reach their peak (Chen et al. 2009; Wang et al. 2013; Yuan et al. 2013). Besides, over the heated continent, the wind diurnal cycles are also found to be evident over the ocean due to the planetary-scale land–sea breeze circulation between the Asian continent and western North Pacific (Huang et al. 2010). Such evident wind diurnal cycles over the land and the ocean are both closely related to the nocturnal rainfall over East Asia (Fujinami et al. 2017; Chen 2020). Therefore, the DMV amplitude is estimated over the southern region of subtropical East Asia where the deviated meridional winds show a summertime maximum, including southern China and a part of the Pacific Ocean (22.5°–35°N, 110°–130°E; the box in Fig. 1a). Because this study focuses on the East Asian regions in the whole summer, the key area for

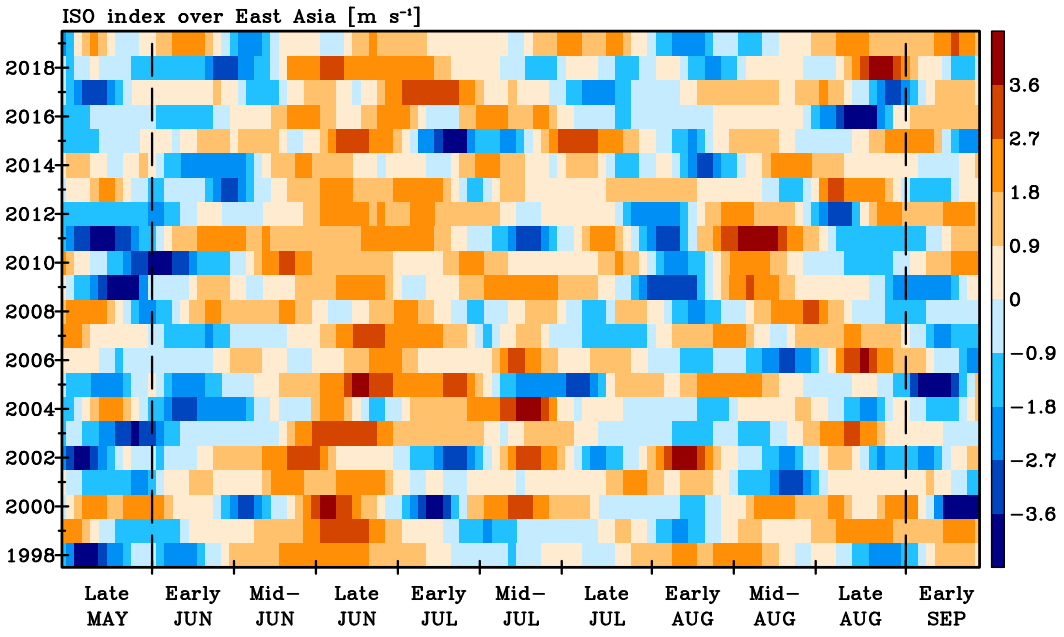

FIG. 2. The 10–90-day ISO index of 925-hPa meridional winds (m s^{-1}).

identification is larger than the key areas in previous studies on the mei-yu–baiu seasons specifically (e.g., Xue et al. 2018; Chen 2020). The days with large DMV amplitudes [namely, DMV(+) days] are identified when the deviated meridional winds averaged at 110°–130°E show a positive anomaly that extends at least 5° of latitude continuously at 22.5°–35°N (Liu et al. 2022). The remaining summer days are considered as the days with small DMV amplitudes [namely, DMV(−) days]. It is noted that the results are insensitive to the key area for identification.

At the intraseasonal time scale (Figs. 1c,d), the ISOs have two dominant periods, namely, the quasi-biweekly/submonthly (10–30-day) mode and the BSISO (30–60-day) mode (Li and Wang 2005; Cao et al. 2017; Wang et al. 2021). The spectrum analysis shows that monsoon southerlies have a significant period of 10–90 days (Fig. S1 in the online supplemental material). In this study, the 10–90-day period is chosen for a time filter to include most of the ISO signals that affect East Asia. The ISO index is estimated as the 10–90-day bandpass-filtered meridional winds averaged in the area (22.5°–30°N, 110°–130°E; the box in Fig. 1c) where the standard deviations of filtered meridional winds maximize in summer. Based on the ISO index, each intraseasonal cycle is divided into eight phases. Phases 3 and 7 denote the period with the strongest anomalous southerlies and northerlies, respectively. Phases 2–4 and phases 6–8 are defined as the southerly and northerly phases of ISOs, respectively. The pronounced ISO activities with a maximum index in the whole period greater than ~1.8 m s^{-1} (0.5 standard deviations above the summer mean) are chosen for statistical analysis. These ISOs are further categorized into two groups based on their amplitudes of DMV. One group is the ISOs with DMV(+), in which the DMV(+) days account for more than 60% of the days in the southerly phases. The other is the remaining ISOs with DMV(−). These two groups of ISOs are compared to clarify the different joint impacts of intraseasonal and diurnal variations on EASM rainfall. To ensure the robustness of the comparisons, we compare the ISO composites based on the two dominant periods and the climatological/transient modes of ISOs (Yang et al. 2010) (Figs. S2 and S3). We also check the ISO composites in the individual months of June–August or in the mei-yu–baiu season and post–mei-yu–baiu season (not shown). The results show that the main conclusions of our study are not sensitive to the detailed types of ISOs categorized by these aspects.

3. Multiscale variabilities of the monsoon southerlies over East Asia

a. *Relationship among the multiscale activities of monsoon southerlies*

As shown in Fig. 2, the values of the ISO index are generally negative before early June. From mid-June to early July, 519 (79%) days are exhibited as positive, indicating the active period of ISOs. Such a seasonally phase-locked manner is associated with climatological ISO (Lau et al. 1988; Song et al. 2016) and corresponds to the northward march of the EASM rain belt from south China to central China and southern Japan (Qian et al. 2002; Wang and LinHo 2002; Ding and Chan 2005). Some values become negative after mid-July when the EASM rain belt is observed over northern China, the Korean Peninsula, and northern Japan. In August, the periods of intraseasonal cycles become short, in which the positive values are related to monsoon revival (Chen et al. 2004). It suggests an evident subseasonal variation of ISO activities and its close relationship with the meridional movement of the EASM.

There are 1367 days with pronounced ISO activities chosen for the statistical analysis, accounting for 68% of the summer

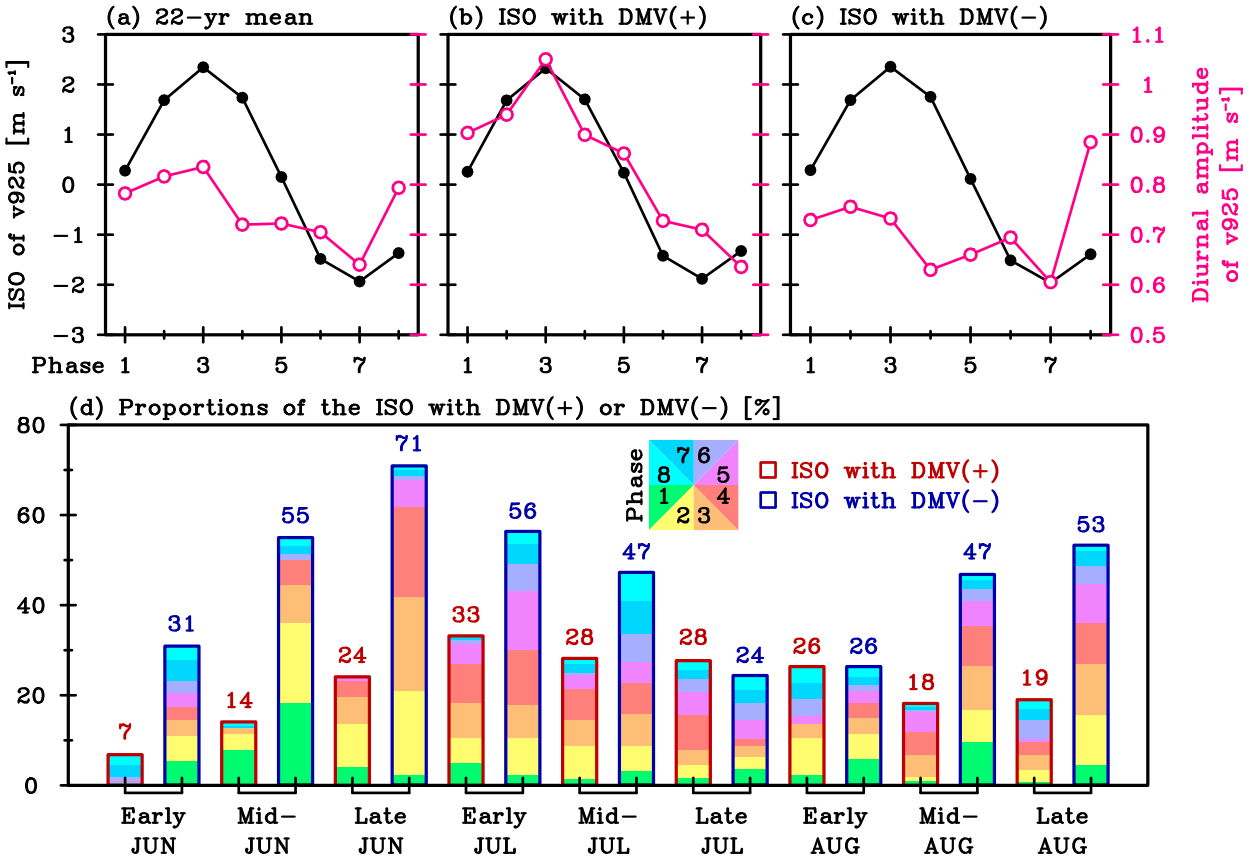

FIG. 3. Components of the 10–90-day ISO index (black; m s^{-1}) and the DMV amplitude (pink; m s^{-1}) averaged over the southern region for (a) the 22-yr summer mean, (b) the ISO with DMV(+), and (c) the ISO with DMV(−). (d) The proportions (%) of the ISOs with DMV(+) or DMV(−) obtained by dividing the summer days in the selected subseasonal period.

days. About 756 (55%) of these days are southerly phases and 278 (20%) of them are northerly phases. These ISOs are further categorized by the diurnal amplitudes of southerlies. The ISOs with DMV(+) include 445 summer days, accounting for about 1/3 of pronounced ISOs, while the ISOs with DMV(−) include the remaining 922 days. The two types of ISOs have different day numbers because we define the ISO with DMV(+) by a relatively restrictive criterion in which DMV(+) days occur in more than 60% of the days in the southerly phases. The two kinds of ISOs appear alternatively in most years, while ISOs with DMV(−) are dominant in some years (1999, 2001–03, and 2012) (Fig. S4). The monsoon southerlies in both kinds of ISOs have similar magnitudes of intraseasonal components to those in the 22-yr summer mean (Figs. 3a–c). They are strongest in phase 3 (2.3 m s^{-1}) and weakest in phase 7 (−1.9 m s^{-1}). The diurnal amplitudes of southerlies in the ISO with DMV(+) are evidently different from those in the ISOs with DMV(−). In the ISO with DMV(+), the diurnal amplitudes increase to the maximum of 1.1 m s^{-1} in phase 3 (much larger than the climate value of 0.8 m s^{-1}) and then gradually decrease to 0.6 m s^{-1} in phase 8. In the ISO with DMV(−), the diurnal amplitudes remain around 0.7 m s^{-1} except for phase 8. In general, the ISOs with DMV(+) have similar intraseasonal components but larger diurnal amplitudes compared with the ISOs with DMV(−). Therefore, the comparison between these two kinds of ISOs can be used to analyze the joint impacts of ISOs with DMVs on East Asian weather and climate.

These two kinds of ISOs also have different subseasonal variations (Fig. 3d). In June, the proportion of the ISO with DMV(−) increases evidently and reaches a maximum of 71%, nearly 3 times the proportion of the ISO with DMV(+) (24%). In early July, the ISOs with DMV(+) have a maximum proportion of 33%, while the ISOs with DMV(−) decrease. The two kinds of ISOs show comparable proportions in late July and early August. In mid- and late August, the ISOs with DMV(−) increase again, but the ISOs with DMV(+) decrease. The DMV amplitudes of ISOs may be related to regional thermal forcings because the ISOs with large DMV amplitudes tend to occur in July when the daytime solar heating is strong over southern China (Zhao et al. 2021), which will be discussed in the following sections. Moreover, the different combinations of ISOs and DMVs may be associated with the EASM rain belt. The frequent ISOs with DMV(−) in June correspond to the mei-yu–baiu season over central China and southern Japan, while the ISOs with DMV(+) in July to the rainy season over northern China, the Korean Peninsula, and northern Japan (Qian et al. 2002;

Wang and LinHo 2002; Ding and Chan 2005). The active ISOs with enhanced precipitation over East Asia have been discussed widely in previous observations (Sun et al. 2016; Lee et al. 2017; Huang et al. 2019; Y. Ding et al. 2021). Recent studies have pointed out that large amplitudes of DMV are favorable for the northward march of the rain belt (Chen 2020; Liu et al. 2022), but it is still unclear how the ISOs and DMVs jointly regulate the monsoon rain belt.

b. *Low-level conditions and rainfall patterns of the ISOs with different DMV amplitudes*

The composites of lower-tropospheric conditions and rainfall responses during the two kinds of ISOs are compared in this subsection. In phase 1 of the ISO with DMV(+), an anomalous anticyclone is generated over the western Pacific (24°N, 141°E) (Fig. 4a). In the southerly phases 2–4, the center of anomalous anticyclone moves northwestward to East Asia (26°N, 131°E) (Figs. 4b–d). At its western flank, the southwesterlies are facilitated extensively with large amplitudes of DMV. The enlargement of DMV accompanies with an anomalous strong warming of up to 2.3 K in the ABL over southern China. In phase 5, the anomalous anticyclone continues to move northwestward (Fig. 4e). The anomalous southwesterlies are maintained over East Asia with weak intensity. When the anomalous anticyclone is dissipated in the northerly phases 6–8, an anomalous cyclone moves from the western Pacific, producing a prevailing anomalous northeasterly over East Asia (Figs. 4f–h).

As for the ISO with DMV(−), an anomalous cyclone is observed over East Asia with anomalous cooling in phase 1 (Fig. 5a). The anomalous anticyclone appears over the western Pacific in phase 2 (Fig. 5b), later than that of the ISO with DMV(+) (Figs. 4a,b). In phases 3–4, it moves westward to East Asia (24°N, 129°E) (Figs. 5c,d), which is located farther south than that of the ISO with DMV(+) (Figs. 4c,d). The anomalous warming is weak over southern China, and the monsoon southwesterlies are confined to the south of 35°N with suppressed DMV amplitudes (Figs. 5c,d). The temperature anomaly to the north of 35°N is still negative with anomalous northeasterlies. In phase 5, the anomalous anticyclone is dissipated (Fig. 5e), which is earlier than that of the ISO with DMV(+) (Fig. 4e). The anomalous cooling is re-established to the south of 35°N (Fig. 5e). In phases 6–8, an anomalous cyclone moves from the western Pacific to East Asia with anomalies of low temperature and prevailing northeasterly winds (Figs. 5f–h). The above results indicate that the active ISOs feature strengthened southerlies at the western flank of a northwestward- or westward-moving anomalous anticyclone. The propagations of anomalous anticyclone seem to regulate the DMV amplitudes in ISOs by modulating both the southwesterly flows and the thermal conditions in the lower troposphere of southern China.

The detailed evolutions of monsoon southerlies during the two kinds of ISOs and their rainfall responses are shown in Fig. 6. In phase 1 of the ISO with DMV(+) (Fig. 6a), anomalous southerlies are observed in the tropics (south of 28°N) with the generation of the anomalous anticyclone (Fig. 4a). In phases 2–4, the anomalous southerlies are strengthened significantly and extended northward to 45°N (Fig. 6a). The in-phase pattern with prevailing anomalous southerlies from the tropics to the midlatitudes corresponds to the northwestward-moving anomalous anticyclone (Figs. 4b–d). In phase 5, the anomalous southerlies are weakened (Fig. 6a). The tropical meridional winds are shown as anomalous northerlies. In phases 6–8, the tropical anomalous northerlies are also extended northward with the approaching anomalous cyclone (Figs. 4f–h). It seems that accompanied by large DMV, the ISO signals over East Asia generally originate from the tropics. As a response, the monsoon rain belt advances northward from central China and southern Japan in phase 1 (Fig. S5) and shows a positive rainfall over northern China and the Korean Peninsula in phases 2–4 (Fig. S6). Such an advance of the positive rainfall anomaly from 28°N to the north of 40°N in the southerly phases indicates a remarkable meridional propagation of the monsoon rain belt (Fig. 6c). In the northerly phases, a negative rainfall anomaly is advanced northward from 26° to 33°N with the extension of anomalous northerlies (Fig. 6a). The rainfall anomaly remains positive at the north of 35°N due to the anomalous easterlies at the northern flank of the anomalous cyclone (Figs. 4f–h). Recent case studies have shown that the easterly winds in the outer regions of tropical cyclones can carry warm moist energy from oceans, which may produce record-breaking rainfall in the midlatitudes during the suppressed phases of ISOs (Huang et al. 2022; Luo and Du 2022; Xu et al. 2022).

In phase 1 of the ISO with DMV(−), anomalous northerlies are observed at 25°–35°N (Fig. 6b) with the anomalous cyclone over East Asia (Fig. 5a). Anomalous southerlies appear in both the tropics (south of 25°N) and the midlatitudes (north of 35°N) (Fig. 6b). In phases 2–4, the tropics-originated anomalous southerlies are extended northward, while the midlatitude-originated ones are propagated southward, implying the combined influence of the circulation systems from the tropics and midlatitudes. The anomalous southerlies are thus confined to the south of 35°N, corresponding to the anomalous anticyclone located farther south than that of the ISO with DMV(+) (cf. Figs. 5b–d and 4b–d). The anomalous southerlies form a dipole pattern with anomalous northerlies to the north of 35°N (Fig. 6b), which is different from the in-phase pattern during the ISO with DMV(+) (Fig. 6a). In phases 5–8, the anomalous northerlies are dominant over East Asia with a southward midlatitude oscillation (Fig. 6b). The rainfall response shows that the positive anomaly is shifted slightly from 28° to 33°N in the southerly phases (Fig. 6d), which is maintained over central China and southern Japan (Fig. S6). The northward propagation of the monsoon rain belt is not as remarkable as that of the ISO with DMV(+) (cf. Figs. 6d and 6c). In phases 5–6, the positive anomaly is established at 37°N (Fig. 6d). It is more significant than the anomalous rainfall in the suppressed phases of the ISO with DMV(+) (Fig. 6c) because of the stronger anomalous easterlies from the anomalous cyclone (cf. Figs. 5e,f and 4f–h). The following negative anomaly of rainfall shows a slight northward propagation to 29°N and disappears in phases 7–8. We also examine the propagation of the monsoon rain belt in the

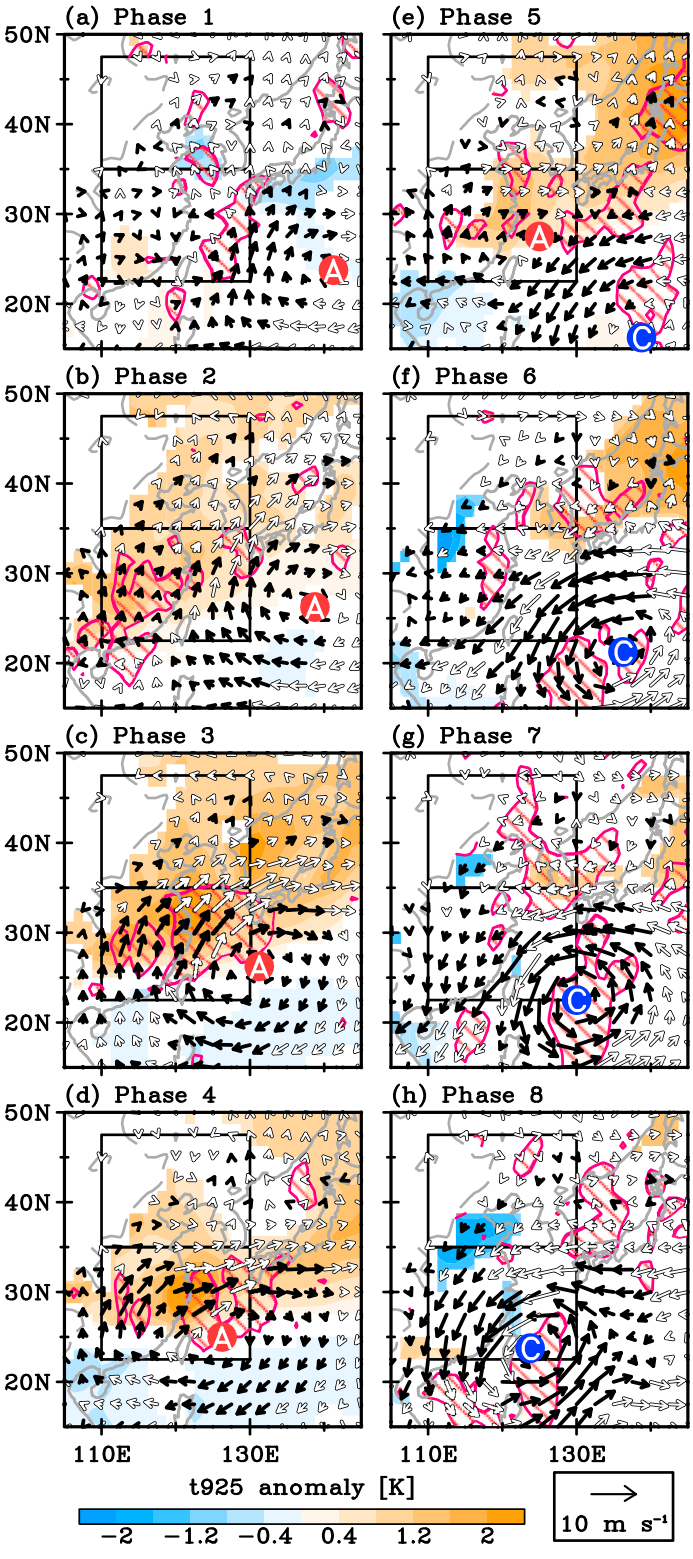

FIG. 4. Daily mean anomalies of winds (vectors; m s^{-1}) and temperature (shading; K; above the 90% confidence level) at 925 hPa during the evolution of the ISO with DMV(+). The black vectors denote the daily mean anomaly of meridional winds above 90% confidence level. The pink hatching denotes the diurnal amplitudes of meridional winds above 0.3 m s^{-1}. The boxes denote the southern region (110°–130°E, 22.5°–35°N) and northern region (110°–130°E, 35°–47.5°N) of subtropical East Asia. The red (blue) circle labeled with "A" ("C") denotes an anomalous anticyclone (cyclone).

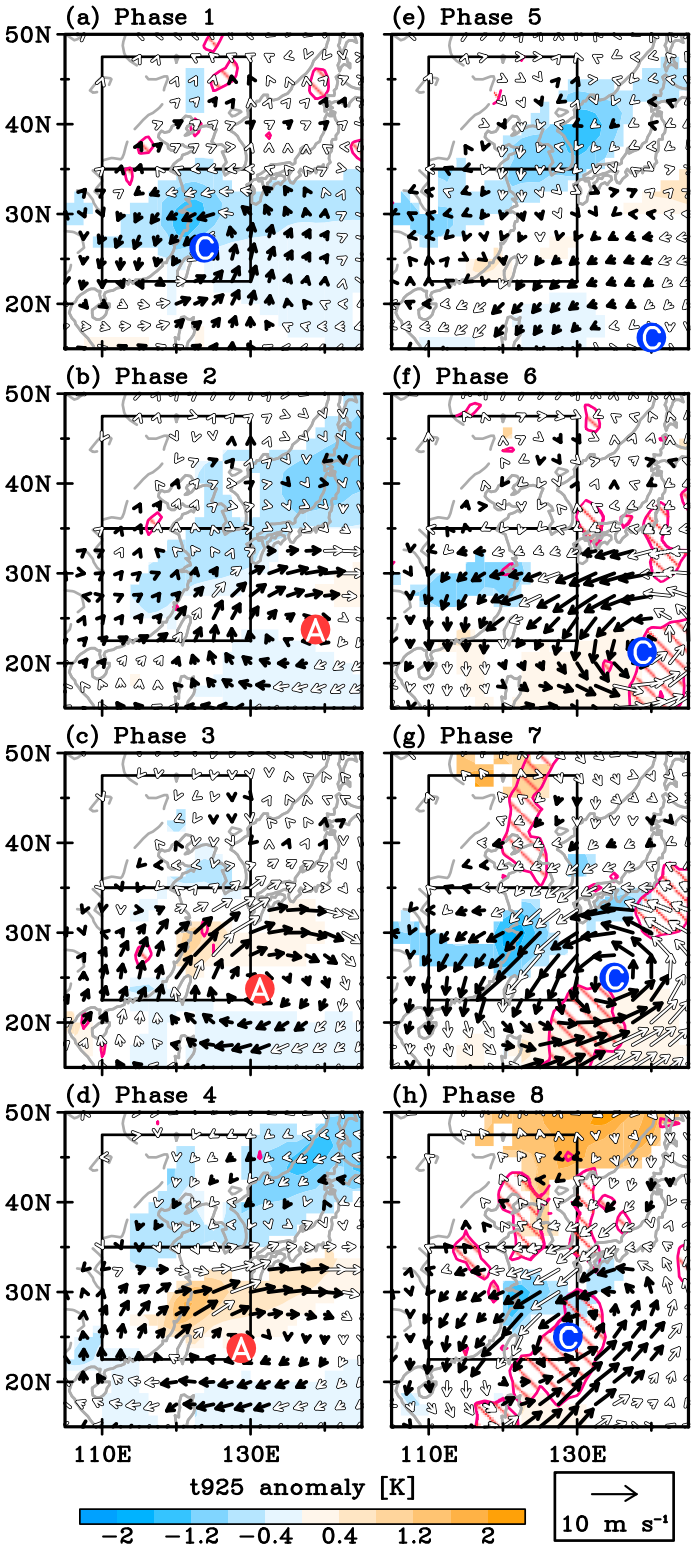

FIG. 5. As in Fig. 4, but for the ISO with DMV(−).

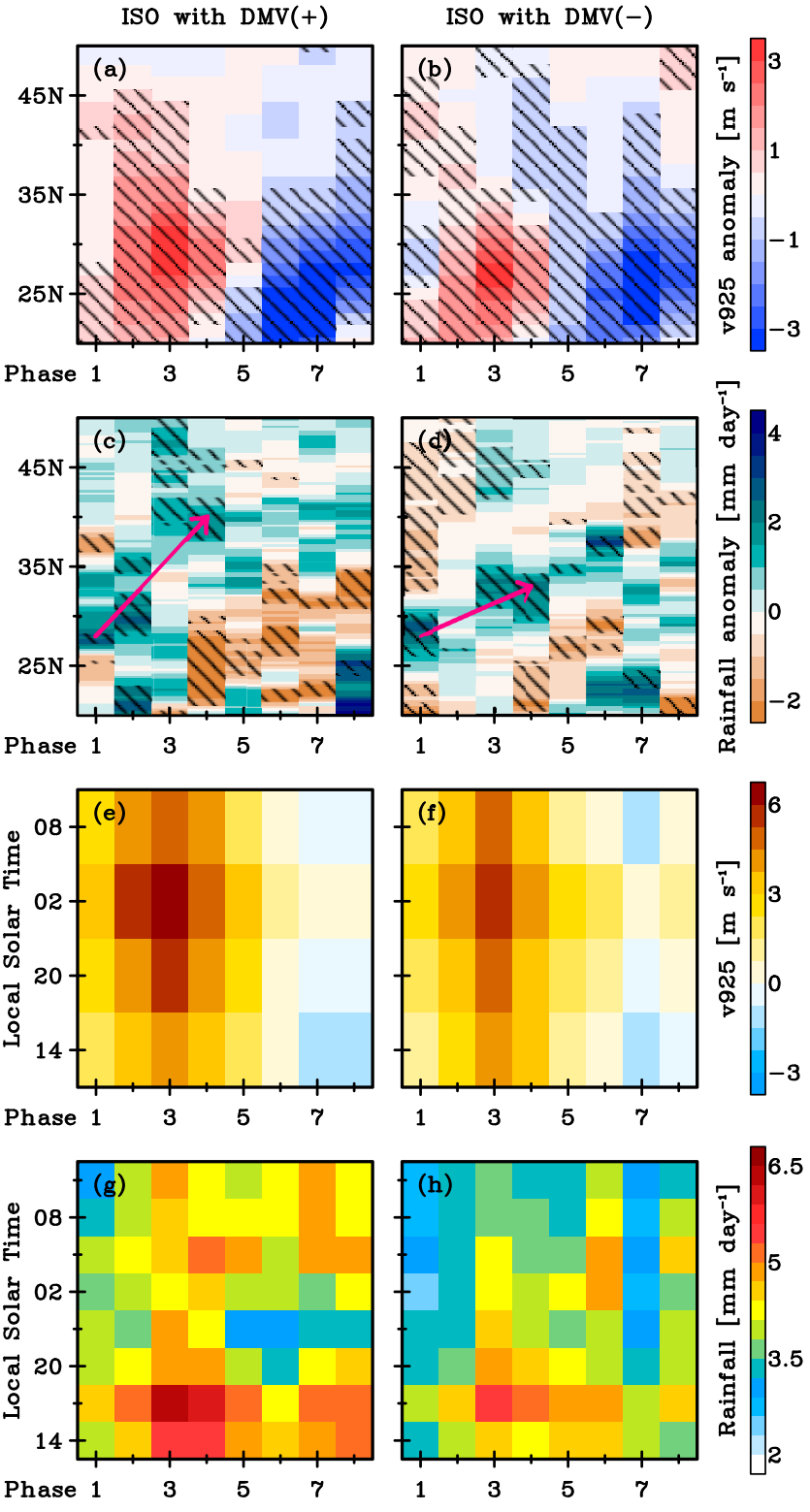

FIG. 6. (a),(b) Anomaly of the daily mean 925-hPa meridional winds (m s^{-1}) averaged at 110°–130°E during the ISO evolutions. The hatching denotes the values above 90% confidence level. (c),(d) As in (a) and (b), but for the daily mean rainfall amounts (mm day^{-1}). The arrows denote the propagations of the monsoon rain belt. (e),(f) Diurnal variations of the meridional winds (m s^{-1}) averaged over the southern region of East Asia (110°–130°E, 22.5°–35°N). (g),(h) As in (e) and (f), but for the rainfall amounts (mm day^{-1}) averaged over the northern region (110°–130°E, 35°–47.5°N).

zonal direction and find that it is not as significant as in the meridional direction (not shown).

The relationship between the DMV amplitudes of ISOs and the meridional propagation of the monsoon rain belt is further examined at the diurnal time scale. During the ISO with DMV(+), the southerlies over the southern region of East Asia (the box at the south of 35°N in Fig. 4) are accelerated at midnight, which have a maximum of 6.4 m s^{-1} at the 0200 LST of phase 3 (Fig. 6e). They intensify the rainfall at their northern terminus, whose daily-mean value over the northern region of East Asia (the box at the north of 35°N in Fig. 4) is increased from 3.8 mm day^{-1} in phase 1 to 4.7 mm day^{-1} in the southerly phases (Fig. 6g). To be specific, the nocturnal acceleration of southerlies largely enhances the rainfall in the midnight to morning hours (0200–1100 LST). The rainfall diurnal variation with a single afternoon peak (1700 LST) in phase 1 is changed to be with two peaks in the afternoon and morning (1100 LST) in the southerly phases.

During the ISO with DMV(−), the southerlies over the southern region are also accelerated at midnight (Fig. 6f), but their maximum (5.5 m s^{-1}) is weaker than that of the ISO with DMV(+) (6.4 m s^{-1}). The intensified daily-mean rainfall over the northern region in the southerly phases (4.0 mm day^{-1}) is less than that of the ISO with DMV(+) (4.7 mm day^{-1}), and the midnight to morning rainfall is weaker (Fig. 6h). Overall, the comparison of Fig. 6 suggests that the ISOs coupled with large DMV tend to exhibit more remarkable northward propagation of the monsoon rain belt with stronger midnight to morning rainfall than those with small DMV. We note that the morning rainfall peaks are present in the northerly phases of both kinds of ISOs, which are produced by the moisture transported by the easterly outflows of cyclones (Fig. S7). The moisture transport is more efficient in nighttime due to the nocturnal LLJs strengthened by the Blackadar and Holton mechanisms (Chen et al. 2013; Luo and Du 2022). It implies two moisture sources for the precipitation in the midlatitude regions of East Asia. One of them is the active monsoon southwesterlies and the other one is the easterly outflows of cyclonic systems when the monsoon flows are suppressed.

4. Large-scale circulations and regional forcings associated with different combinations of ISO and DMV

a. Large-scale circulations during the evolutions of ISOs

The above composite analyses show that the two kinds of ISOs may evolve with different large-scale circulations, especially the influences of tropical and midlatitude systems. The middle-level geopotential height at 500 hPa during the evolutions of ISOs is shown in Fig. 7. In phase 1 of the ISO with DMV(+), the WPSH (refer to the 5880-gpm contours) is observed at the east of 130°E with an anomalous high over the western Pacific (24°N, 140°E) (Fig. 7a). In phases 2–4, the WPSH extends westward to 119°E with a north–south extent of 18° at 130°E (Figs. 7b–d). The anomaly of geopotential height moves northwestward to East Asia (31°N, 128°E) and is strengthened to 35 gpm, corresponding to the northwestward anomalous anticyclone in the lower level (Figs. 4b–d). Meanwhile, the geopotential height is also positive in the midlatitudes (Figs. 7b–d), which is conducive to the in-phase pattern with anomalous southerlies (Fig. 6a). In phase 5, the anomaly of geopotential height continuously moves northward to the mid–high latitudes of the westerlies although the WPSH in the lower latitudes retreats eastward (Fig. 7e). In phases 6–8, the anomalous high in the westerlies moves eastward to the east of Japan and an anomalous low moves northwestward from the western Pacific to East Asia (Figs. 7f–h) with a low-level anomalous cyclone (Figs. 4f–h).

In contrast, a deep westerly trough with an anomalous low is seen over East Asia in phase 1 of the ISO with DMV(−) (Fig. 7i), which is related to the low-level anomalous cyclone (Fig. 5a). Confined by the westerly trough, the WPSH extends westward to 123°E with a north–south extent of 10° at 130°N in phases 2–4, which is weaker than that during the ISO with DMV(+) (cf. Figs. 7j–l and 7b–d). The following anomalous high also moves westward with a weaker intensity (20 gpm) and a farther south location (25°N, 129°E). It forms a dipole pattern with the anomalous low in the mid–high-latitude westerlies, which is different from the in-phase pattern during the ISO with DMV(+). Such a dipole pattern of anomalous geopotential height contributes to the dipole pattern of anomalous meridional winds in the lower troposphere (Fig. 6b). In phase 5, the anomalous high moves westward and is weakened over southeastern China with the eastward retreat of the WPSH (Fig. 7m). The dipole pattern of anomalous geopotential height is reversed in phases 6–8 (Figs. 7n–p). It seems that the dipole pattern during the ISO with DMV(−) is related to the combined influences of the tropical and midlatitude signals, in sharp contrast with the in-phase pattern with the dominant northwestward-moving tropical signal during the ISO with DMV(+).

Figure 8 shows the coupling of the upper-level circulations with a focus on the southerly phases. During the ISO with DMV(+), the eastern ridge of the South Asian high (SAH) (red dot at the 12 520-gpm contour) is located to the northeast of the climate mean (green dot) (Fig. 8a). This northeastward expansion of the SAH is related to an extensively positive anomaly of geopotential height over East Asia. It is also characterized by anomalous upper-level divergence, facilitating the dynamic lifting for the northwestward propagation of low-level ISOs (Figs. 4b–d). During the ISO with DMV(−), the eastward expansion of the SAH is small (Fig. 8b). The anomaly of geopotential height is positive to the south of 35°N and negative to the north of 35°N. The dipole pattern similar to the middle-level one shows the coexistence of the tropical and midlatitude systems. The anomalous upper-level divergence is confined to the southern region. Previous studies suggested that the variations of the SAH are sensitive to the landmass thermal conditions (Duan and Wu 2005; Wu et al. 2007). The different expansions of the SAH during the two kinds of ISO with large or small DMV may be associated with the differences in tropospheric temperature by the expansion of air column (cf. the shadings in Figs. 4 and 5).

This subsection shows that the large-scale circulations have in-phase patterns between low and middle latitudes during the ISO with DMV(+) but dipole patterns during the ISO with DMV(−). It implies that the ISOs have a barotropic structure and their evolutions are jointly modulated by the

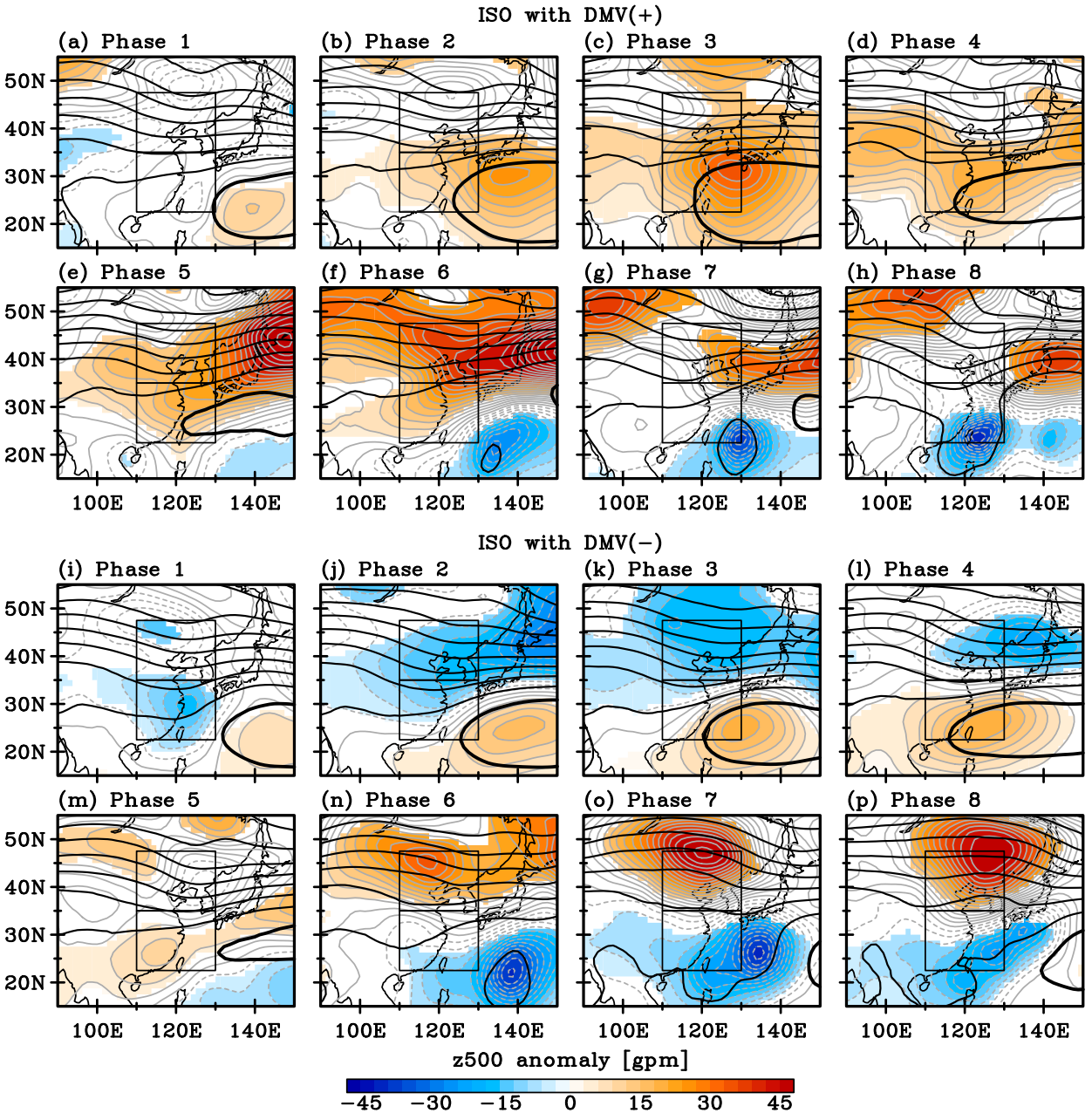

FIG. 7. Geopotential height at 500 hPa (black contours with intervals of 30 gpm; thick contours denote the 5880-gpm lines) and its anomaly (gray contours with intervals of 3 gpm; shading denotes the values above the 90% confidence level).

tropical and midlatitude circulation systems. Specifically, the ISOs with large DMV amplitudes are characterized by the simultaneous expansions of the WPSH and SAH, while those with small DMV amplitudes are related to the active westerly trough coupled with the relatively weak WPSH and SAH.

b. *Impacts of regional thermal forcings on the DMV amplitudes of ISOs*

The diurnal amplitudes of low-level winds are efficiently regulated by the thermally driven ABL turbulent mixing (Xue et al. 2018; Chen 2020), which may be represented by the diurnal variation of vertical structure of potential temperature (Fujinami et al. 2022) and the diurnal range of 925-hPa temperature (Wu et al. 2023). A high correlation between the diurnal range of 925-hPa temperature and the diurnal cycle of monsoon southerly is observed over East Asia (Wu et al. 2023). In this study, we further examine the diurnal range of 925-hPa temperature from 0800 to 2000 LST in the southerly phases to clarify the couplings of ISOs with different regional-scale thermal forcings. Figure 9 shows that the local change of ABL temperature ($\partial T/\partial t$) is up to 3.7 K during the ISO with

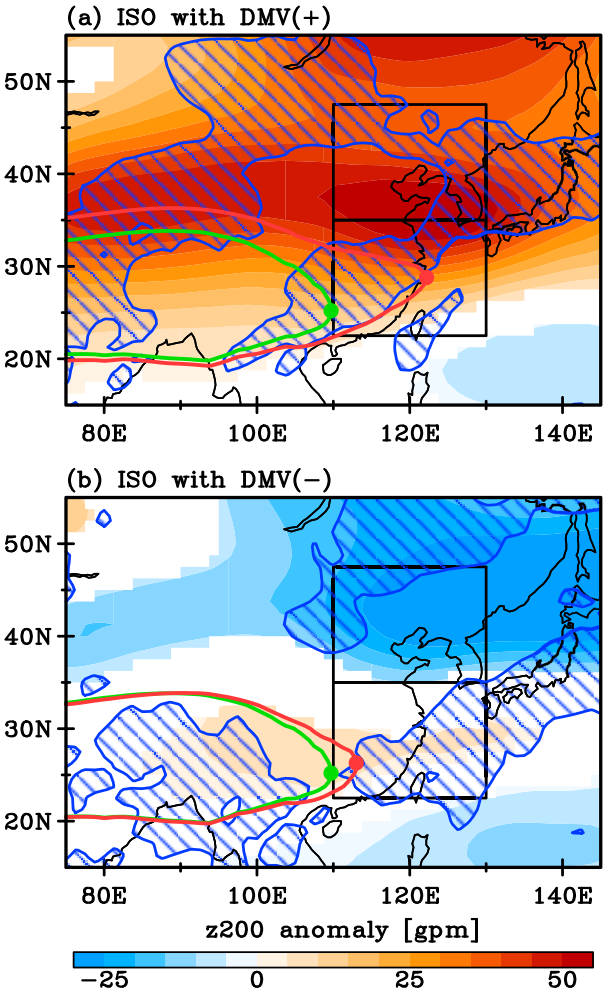

FIG. 8. Anomalies of the geopotential height (shading; gpm; above the 90% confidence level) and divergence (hatching; above 10^{-6} s^{-1}) in the southerly phases of (a) the ISO with DMV(+) and (b) the ISO with DMV(−). The red and green contours denote the 12 520-gpm lines of the 200-hPa geopotential height and their climate-mean state, respectively. The dots denote the easternmost point of the contours.

DMV(+), which is greater than that during the ISO with DMV(−) (2.8 K) (Figs. 9a–c). It agrees with the discussion in section 3b that large DMV amplitudes of ISOs tend to occur with a warm boundary layer. It also explains why the ISOs with DMV(+) are mostly observed in July when the solar heating is strong (Fig. 3d).

To investigate the relative contribution of different physical processes, the local change of temperature is decomposed into the rates by diabatic heating (Q) as well as the advections in the zonal ($-u\partial T/\partial x$), meridional ($-v\partial T/\partial y$), and vertical ($-w\partial T/\partial z$) directions. The diabatic heating is observed as the largest positive value (Figs. 9d,e). The diabatic heating consists of sensible heating from solar radiation and latent heating from precipitation. Over southern China, the daytime solar radiation is dominant in the boundary layer as it strongly heats surface and contributes to the emitted sensible heat flux, while the release of latent heating due to condensation is relatively small. The values of zonal advection are negative over the landmass and positive over the sea (Figs. 9g,h), which is attributed to the westerly component of monsoon flows that convey warm air masses from land to sea. The values of meridional advection are negative south of 30°N and positive north of 30°N (Figs. 9j,k), suggesting a northward transport of warm air mass by monsoon southerlies. The values of vertical advection are generally negative near 25°N (Figs. 9m,n), which means a downward transport of cool air masses from the upper level. As a whole, the thermal differences between the two kinds of ISOs are primarily produced by diabatic heating (Figs. 9f,i,l,o). The weather states with less cloudiness during the DMV(+) days with enhanced WPSH are more favorable for solar radiation heating than those during the DMV(−) days (Wu et al. 2023). There is extensive literature on the relationship of different tropical ISO propagations with oceanic background states (e.g., Wang et al. 2021; Wei et al. 2023). We further highlight that the two kinds of ISOs over East Asia actually represent the large-scale conditions that are coupled with the different regional thermal forcings at diurnal time scales and relevant DMV amplitudes.

5. Physical mechanisms governing rainfall during ISOs with different DMV amplitudes

It has been widely documented that active monsoon flows are crucial for producing rainfall patterns in the summertime through modulating dynamic lifting and moisture budget (e.g., X. Chen et al. 2017; Fujinami et al. 2017; Chen 2020; Liu et al. 2022). In this section, the modulation effect by the ISOs with large or small DMV will be analyzed with more attention to their influences on the meridional propagation of the monsoon rain belt.

a. *Dynamic lifting*

Figure 10 shows the variations of dynamic conditions at intraseasonal and diurnal time scales. During the ISO with DMV(+), the daily-mean ascending motions at 700 hPa are strengthened to -1.2×10^{-2} Pa s^{-1} in the southerly phases (Fig. 10a), guiding the rain belt northward (Fig. 6c). They are changed to descending motions in the northerly phases (Fig. 10a). The daily-mean ascending motions in the southerly phases are contributed by the components at midnight (0200 LST) and afternoon (1400 LST), matching the double peaks of rainfall over the northern region (Fig. 6g). The ascending motions at midnight are pronounced and reach a peak of -2.0×10^{-2} Pa s^{-1} in phase 3. They are facilitated by the convergence of monsoon southerlies at 925 hPa, whose midnight components have a peak of -3.1×10^{-6} s^{-1} in phase 3 (Fig. 10b). In contrast, the low-level convergence is weakest in the afternoon when the monsoon southerlies attain a diurnal minimum (Yu et al. 2009; Chen et al. 2013). Previous studies noted that daytime surface heating can produce short-duration precipitation systems with a peak at 1700 LST (Fig. 6g; Luo et al. 2013; Li et al. 2020; Liu et al. 2022), which may induce the afternoon ascending motions (Fig. 10a).

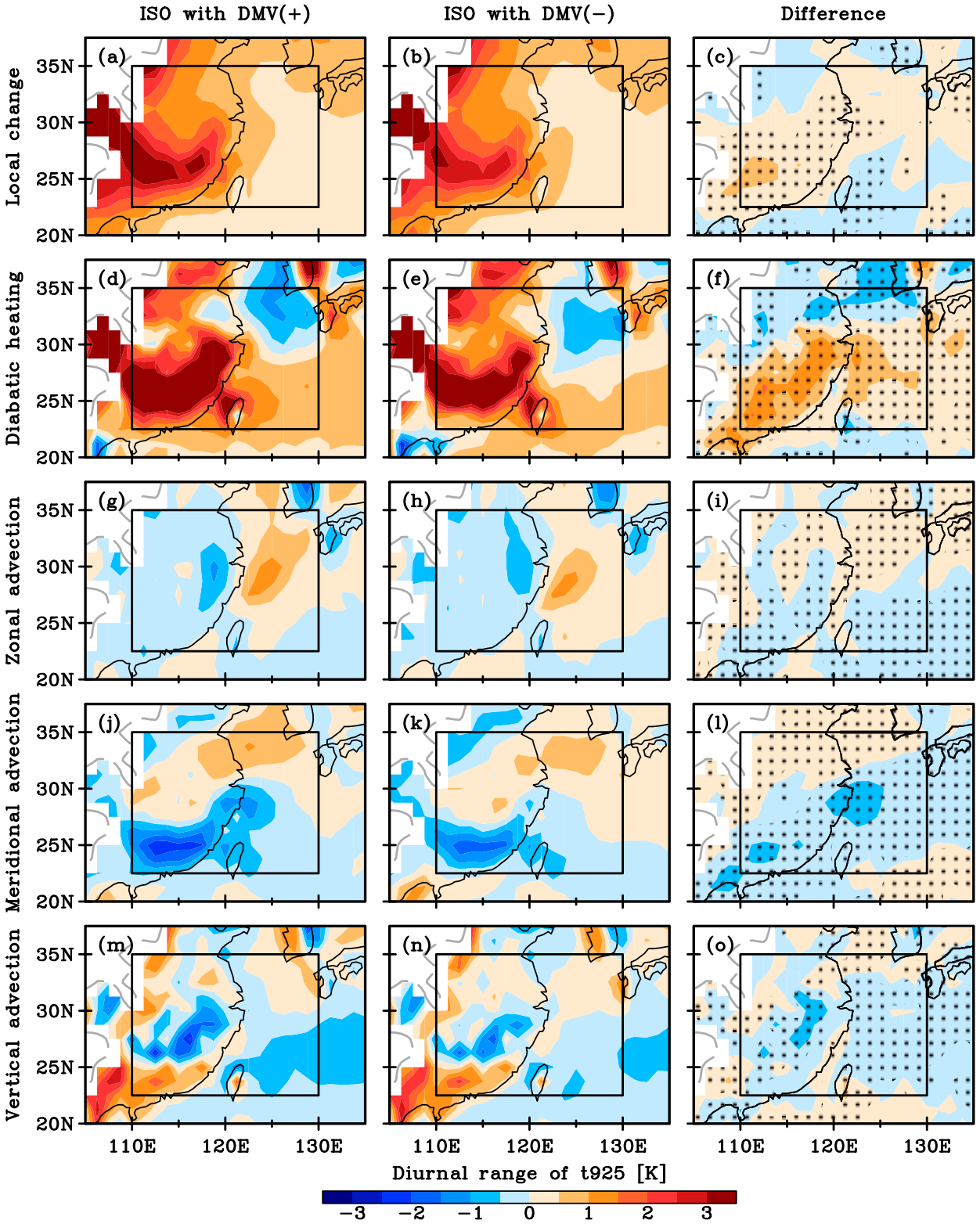

FIG. 9. Diurnal range of the 925-hPa temperature (K) at 0800–2000 LST by different physical processes in the southerly phases of (left) the ISO with DMV(+) and (center) the ISO with DMV(−). (right) The difference between the ISO with DMV(+) and the ISO with DMV(−). The dots denote the values above 90% confidence level.

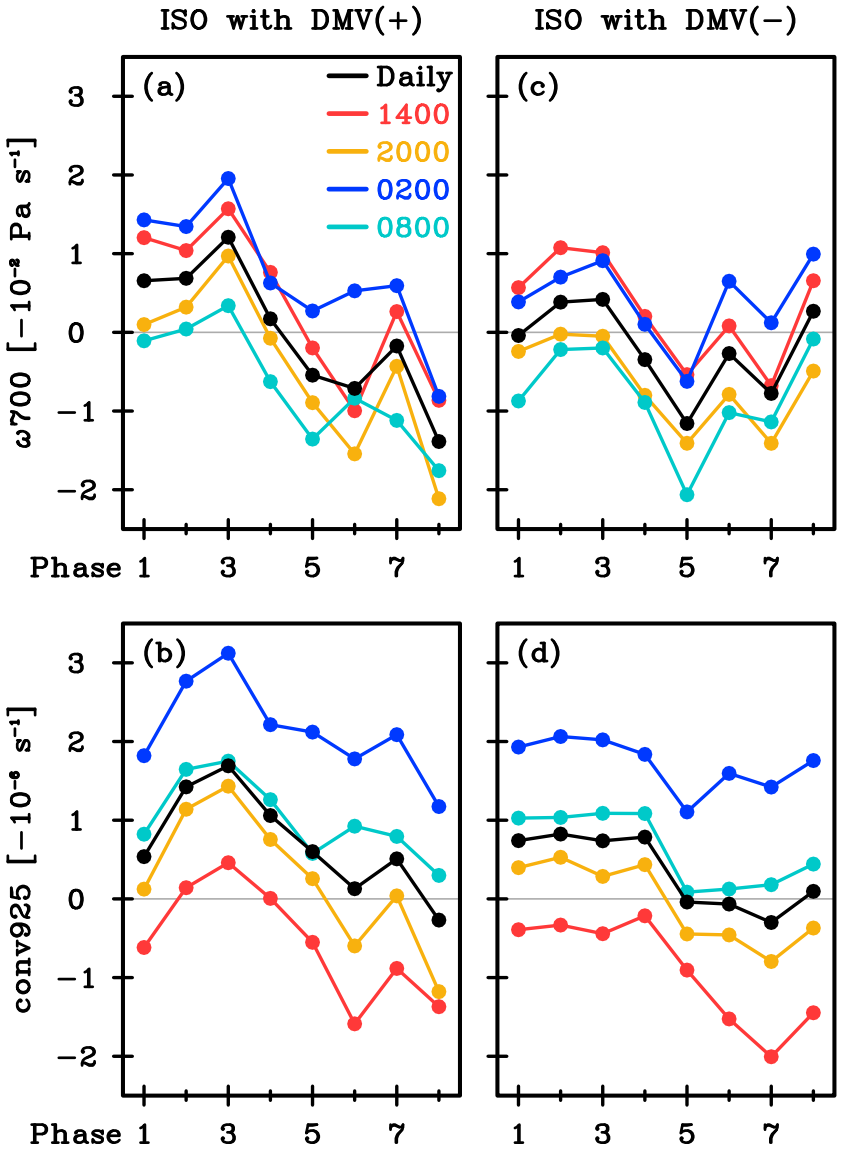

FIG. 10. Diurnal variations of (a),(c) 700-hPa vertical motions and (b),(d) 925-hPa convergence averaged over the northern region during the ISO evolutions.

During the ISO with DMV(−), the daily-mean ascending motions reach a peak of -0.4×10^{-2} Pa s^{-1} in phase 3 (Fig. 10c), which is only 35% of the peak of the ISO with DMV(+) (-1.2×10^{-2} Pa s^{-1}). They are too weak to establish the rain belt over the northern region (Fig. 6d). The weak daily-mean ascending motions are largely attributed to the weak midnight components (Fig. 10c), whose peak is -0.9×10^{-2} Pa s^{-1}, 47% of that during the ISO with DMV(+) (-2.0×10^{-2} Pa s^{-1}). The midnight values of low-level convergence are weaker than -2.1×10^{-6} s^{-1} (Fig. 10d). Such a lifting condition at midnight is consistent with the weak rainfall in the midnight to morning hours (Fig. 6h). It indicates that in the southerly phases of ISOs, monsoon southerlies with different DMV amplitudes can strongly regulate low-level convergence and dynamic lifting at their northern terminus for the northward advance of the rain belt.

b. *Moisture budget*

Besides the differences in lifting conditions, the ISOs with different DMV amplitudes also have different influences on moisture transport, as shown in Fig. 11. During the ISO with DMV(+), the daily-mean meridional fluxes of water vapor at 35°N (the southern boundary of the northern region) are increased evidently in the southerly phases with a maximum of 150.9 kg m^{-1} s^{-1} (Fig. 11a). It is mainly induced by the increase of midnight components with the enhancement of nocturnal southerly acceleration. The midnight components have a maximum of 178.3 kg m^{-1} s^{-1}, 18% greater than that of the daily-mean values, while the components at other hours are less than the daily-mean values. Due to the sufficient inflows of water vapor, the daily-mean moisture convergence over the northern region is strengthened to -3.3×10^{-5} kg m^{-2} s^{-1} in

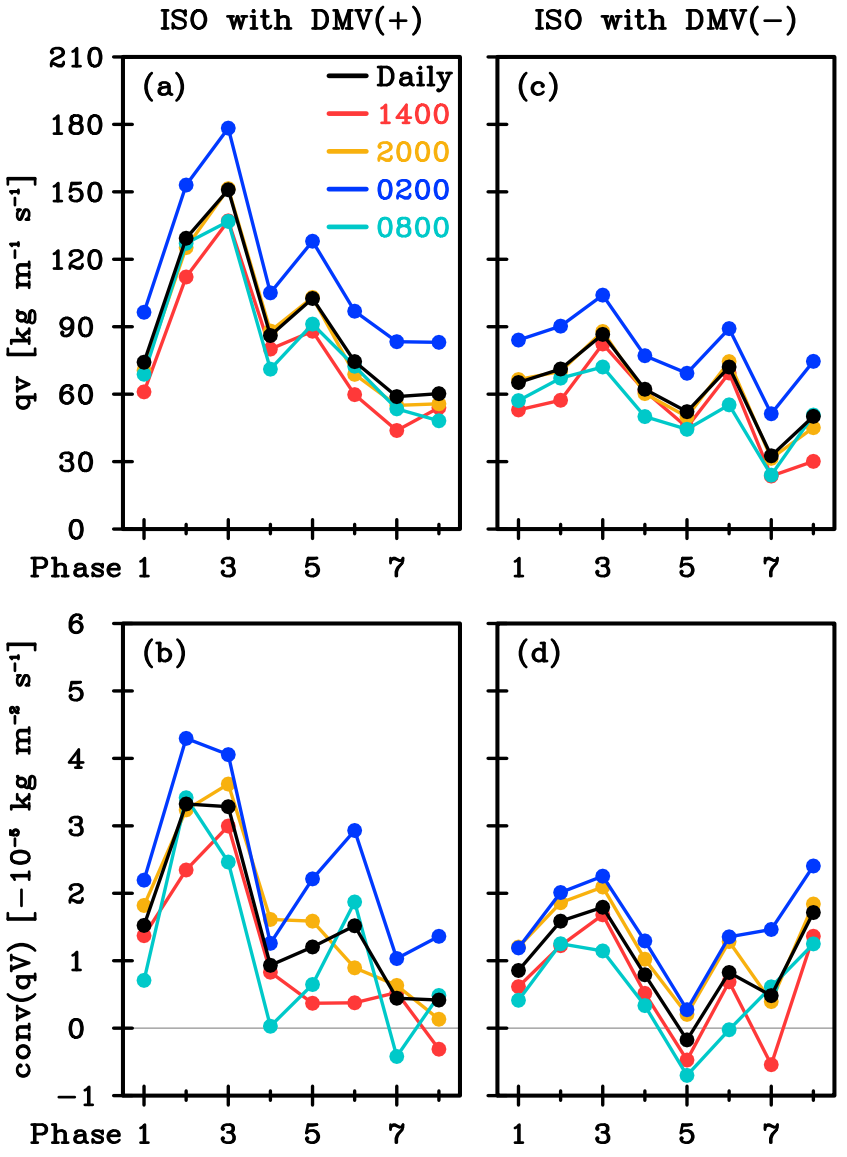

FIG. 11. Diurnal variations of column-integrated (a),(c) meridional water vapor flux at 35°N and (b),(d) water vapor convergence averaged over the northern region during the ISO evolutions.

phase 3 (Fig. 11b), in association with the remarkable northward advance of the rain belt (Fig. 6c). The high daily-mean values are also attributed to the midnight components that is -4.1×10^{-5} kg m^{-2} s^{-1} in phase 3 (Fig. 11b), producing the pronounced precipitation in the midnight to morning hours (Fig. 6g). It is noted that compared with phase 3, the moisture convergence in phase 2 is greater because the divergence of the zonal component is weaker (not shown).

As a comparison, the daily-mean meridional fluxes at 35°N during the ISO with DMV(−) have a maximum of 86.6 kg m^{-1} s^{-1} (Fig. 11c), only 57% of that during the ISO with DMV(+) (150.9 kg m^{-1} s^{-1}). It is related to the weak midnight components with a maximum of 104.1 kg m^{-1} s^{-1} owing to the monsoon southerlies with small DMV amplitudes. The moisture inflows induce a convergence of water vapor with a daily mean of -1.8×10^{-5} kg m^{-2} s^{-1} and a midnight component of -2.3×10^{-5} kg m^{-2} s^{-1} in phase 3 (Fig. 11d). Both of them are much weaker than those during the ISO with DMV(+) (-3.3×10^{-5} and -4.1×10^{-5} kg m^{-2} s^{-1}). Correspondingly, the rain belt is not established over the northern region with less midnight to morning rainfall (Figs. 6d,h). In brief, active ISOs coupled with large DMV are more effective in providing dynamic and moisture conditions with a warm boundary layer (cf. the shadings in Figs. 4 and 5), enhancing convective instability for the northward advance of the rain belt.

6. Conclusions and discussion

In this study, we compare the ISOs with DMV(+) and those with DMV(−) in the past 22-yr summers of 1998–2019

to clarify the joint impacts of ISOs and diurnal cycles on summer rainfall. In particular, we examine the two types of ISOs with emphasis on the different couplings of large-scale circulations and regional forcings. We also estimate their different modulation on the physical processes that are associated with the meridional movements of the EASM rain belt. The major findings are summarized as follows:

1) The ISOs with DMV(+) have similar intraseasonal components but larger diurnal amplitudes of southerlies at 0200 LST compared with the ISOs with DMV(−). The accelerated southerlies at the midnight of ISOs with DMV(+) intensify midnight to morning rainfall and help the rain belt propagate northward remarkably to the north of 40°N. During ISOs with DMV(−), the nocturnal southerly acceleration and nighttime rainfall are weaker. The monsoon rain belt tends to propagate northward in the southerly phases of both kinds of ISOs, but the northward shift is much more pronounced in the ISOs with DMV(+). The different precipitation responses to the two types of ISOs also correspond to the subseasonal variations of the EASM rain belt.
2) The combination of ISOs with DMVs represents the coupling of large-scale circulations with subdaily regional-scale forcings. Active ISOs with DMV(+) feature strengthened southerlies at the western flank of a northwestward-moving anomalous anticyclone. Such a dominant tropical signal is related to the simultaneous expansions of the WPSH and SAH, which produces an in-phase anomalous pattern of geopotential height between the low and middle latitudes over East Asia. This pattern is conducive to the anomalous ABL heating over southern China by daytime solar radiation, facilitating an increase in the diurnal amplitudes of monsoon southerlies. In contrast, the anomalous anticyclone moves westward during ISOs with DMV(−). They are regulated by both tropical and midlatitude signals, in which the WPSH and SAH have relatively small expansions and the westerly trough is active in the midlatitudes. The large-scale conditions lead to a dipole pattern of geopotential height anomaly with the relatively weak regional thermal forcings over East Asia that are related to the small diurnal cycle of southerlies.
3) The active ISOs improve dynamic and moisture conditions for precipitation, while their couplings with DMVs can further regulate these atmospheric processes at the diurnal time scale. During the active ISOs with DMV(+), the enhanced monsoon southerlies at midnight carry abundant water vapor and converge at their northern terminus effectively. They help to establish convective instability in a warm moist ABL for producing midnight to morning rainfall, thereby inducing a remarkable northward shift of the rain belt. During the ISOs with DMV(−), both dynamic lifting and moisture conditions are relatively weak, and the induced rain belt is located farther south.

The ISO propagations have an important influence on the weather and climate over East Asia (Ding and Wang 2008; Song et al. 2016; Cheng et al. 2020, 2021; Wang et al. 2023), and the wind diurnal cycles greatly modulate the spatiotemporal rainfall patterns (Xue et al. 2018; Chen 2020; Guan et al. 2020). Recent studies found that they are closely related to each other in the tropics (e.g., Chen et al. 2019; Natoli and Maloney 2019; Chudler et al. 2020; Xu et al. 2021). This study, for the first time, shows that the couplings of intraseasonal and diurnal atmospheric oscillations are also robust over extratropical East Asia. The ISO-related large-scale conditions are coupled with regional-scale diurnal forcings in different manners so that they jointly modulate the activities of summer rainfall. We note that some issues need further investigation. For instance, the rain belt remains at the north of 35°N in the northerly phases of ISOs with different moisture transport pathways compared with those in the southerly phases. The comparison should be clarified in detail, although it is beyond the scope of this study. Moreover, the ISO propagations have been linked to the steady changes in tropical air–sea interaction (Zheng and Huang 2019; Yang et al. 2020; Wang et al. 2021; Wei et al. 2023). They may be also associated with the land–atmosphere interaction over the extratropical landmass. Our study indicates the downscale connection from large-scale conditions to regional-scale diurnal forcings, while the possible upscale feedback of DMV and ISO to background conditions is an interesting topic for future research. More studies on these short-term precursors of regional climate in both intraseasonal and diurnal time scales would help the prevention and mitigation of natural disasters over densely populated East Asia.

Acknowledgments. The authors are grateful to the Japan Meteorological Agency for providing the Japanese 55-year Reanalysis (JRA-55) and to the NASA Goddard Space Flight Center for providing the TRMM rainfall data. The authors also thank the editor, Professor Pang-chi Hsu, and three anonymous reviewers for their constructive suggestions. This work was supported by the Guangdong Major Project of Basic and Applied Basic Research (2020B0301030004) and National Natural Science Foundation of China (Grant 41575068).

Data availability statement. The JRA-55 data are available from JMA at https://jra.kishou.go.jp/JRA-55/index_en.html. The TRMM rainfall data are available at https://gpm.nasa.gov/data-access/downloads/trmm.

REFERENCES

Blackadar, A. K., 1957: Boundary-layer wind maxima and their significance for the growth of nocturnal inversions. *Bull. Amer. Meteor. Soc.*, **38**, 283–290, https://doi.org/10.1175/1520-0477-38.5.283.

Cao, X., R. Wu, and S. Chen, 2017: Contrast of 10–20-day and 30–60-day intraseasonal SST propagation during summer and winter over the South China Sea and western North Pacific. *Climate Dyn.*, **48**, 1233–1248, https://doi.org/10.1007/s00382-016-3138-z.

Chang, C.-P., R. H. Johnson, K.-J. Ha, D. Kim, G. N.-C. Lau, B. Wang, M. M. Bell, and Y. Luo, 2018: The multiscale global monsoon system: Research and prediction challenges in weather and climate. *Bull. Amer. Meteor. Soc.*, **99**, ES149–ES153, https://doi.org/10.1175/BAMS-D-18-0085.1.

Chen, G., 2020: Diurnal cycle of the Asian summer monsoon: Air pump of the second kind. *J. Climate*, **33**, 1747–1775, https://doi.org/10.1175/JCLI-D-19-0210.1.

——, W. Sha, and T. Iwasaki, 2009: Diurnal variation of precipitation over southeastern China: 2. Impact of the diurnal monsoon variability. *J. Geophys. Res.*, **114**, D21105, https://doi.org/10.1029/2009JD012181.

——, ——, M. Sawada, and T. Iwasaki, 2013: Influence of summer monsoon diurnal cycle on moisture transport and precipitation over eastern China. *J. Geophys. Res. Atmos.*, **118**, 3163–3177, https://doi.org/10.1002/jgrd.50337.

——, T. Iwasaki, H. Qin, and W. Sha, 2014: Evaluation of the warm-season diurnal variability over East Asia in recent reanalyses JRA-55, ERA-Interim, NCEP CFSR, and NASA MERRA. *J. Climate*, **27**, 5517–5537, https://doi.org/10.1175/JCLI-D-14-00005.1.

——, W. Sha, T. Iwasaki, and Z. Wen, 2017: Diurnal cycle of a heavy rainfall corridor over East Asia. *Mon. Wea. Rev.*, **145**, 3365–3389, https://doi.org/10.1175/MWR-D-16-0423.1.

——, Y. Du, and Z. Wen, 2021: Seasonal, interannual, and interdecadal variations of the East Asian summer monsoon: A diurnal-cycle perspective. *J. Climate*, **34**, 4403–4421, https://doi.org/10.1175/JCLI-D-20-0882.1.

Chen, R., Z. Wen, and R. Lu, 2018: Large-scale circulation anomalies and intraseasonal oscillations associated with long-lived extreme heat events in south China. *J. Climate*, **31**, 213–232, https://doi.org/10.1175/JCLI-D-17-0232.1.

Chen, T.-C., and K. Takahashi, 1995: Diurnal variation of outgoing longwave radiation in the vicinity of the South China Sea: Effect of intraseasonal oscillation. *Mon. Wea. Rev.*, **123**, 566–577, https://doi.org/10.1175/1520-0493(1995)123<0566:DVOOLR>2.0.CO;2.

——, S.-Y. Wang, W.-R. Huang, and M.-C. Yen, 2004: Variation of the East Asian summer monsoon rainfall. *J. Climate*, **17**, 744–762, https://doi.org/10.1175/1520-0442(2004)017<0744:VOTEAS>2.0.CO;2.

Chen, X., F. Zhang, and K. Zhao, 2017: Influence of monsoonal wind speed and moisture content on intensity and diurnal variations of the mei-yu season coastal rainfall over South China. *J. Atmos. Sci.*, **74**, 2835–2856, https://doi.org/10.1175/JAS-D-17-0081.1.

——, ——, and J. H. Ruppert Jr., 2019: Modulations of the diurnal cycle of coastal rainfall over South China caused by the boreal summer intraseasonal oscillation. *J. Climate*, **32**, 2089–2108, https://doi.org/10.1175/JCLI-D-18-0786.1.

Cheng, Y., L. Wang, and T. Li, 2020: Causes of interdecadal increase in the intraseasonal rainfall variability over southern China around the early 1990s. *J. Climate*, **33**, 9481–9496, https://doi.org/10.1175/JCLI-D-20-0047.1.

——, ——, and ——, 2021: Two distinct types of 10–30-day persistent heavy rainfall events over the Yangtze River Valley. *J. Climate*, **34**, 9571–9584, https://doi.org/10.1175/JCLI-D-20-0741.1.

Chow, K. C., and J. C. L. Chan, 2009: Diurnal variations of circulation and precipitation in the vicinity of the Tibetan Plateau in early summer. *Climate Dyn.*, **32**, 55–73, https://doi.org/10.1007/s00382-008-0374-x.

Chudler, K., W. Xu, and S. A. Rutledge, 2020: Impact of the boreal summer intraseasonal oscillation on the diurnal cycle of precipitation near and over the island of Luzon. *Mon. Wea. Rev.*, **148**, 1805–1827, https://doi.org/10.1175/MWR-D-19-0252.1.

Ding, L., T. Li, and Y. Sun, 2021: Subseasonal and synoptic variabilities of precipitation over the Yangtze River Basin in the summer of 2020. *Adv. Atmos. Sci.*, **38**, 2108–2124, https://doi.org/10.1007/s00376-021-1133-8.

Ding, Y., and J. C. L. Chan, 2005: The East Asian summer monsoon: An overview. *Meteor. Atmos. Phys.*, **89**, 117–142, https://doi.org/10.1007/s00703-005-0125-z.

——, and Z. Wang, 2008: A study of rainy season in China. *Meteor. Atmos. Phys.*, **16**, 121–138, https://doi.org/10.1007/s00703-008-0299-2.

——, Y. Liu, and Z.-Z. Hu, 2021: The record-breaking Mei-Yu in 2020 and associated atmospheric circulation and tropical SST anomalies. *Adv. Atmos. Sci.*, **38**, 1980–1993, https://doi.org/10.1007/s00376-021-0361-2.

Duan, A. M., and G. X. Wu, 2005: Role of the Tibetan Plateau thermal forcing in the summer climate patterns over subtropical Asia. *Climate Dyn.*, **24**, 793–807, https://doi.org/10.1007/s00382-004-0488-8.

Fu, P., K. Zhu, K. Zhao, B. Zhou, and M. Xue, 2019: Role of the nocturnal low-level jet in the formation of the morning precipitation peak over the Dabie Mountains. *Adv. Atmos. Sci.*, **36**, 15–28, https://doi.org/10.1007/s00376-018-8095-5.

Fujinami, H., and T. Yasunari, 2009: The effects of midlatitude waves over and around the Tibetan Plateau on submonthly variability of the East Asian summer monsoon. *Mon. Wea. Rev.*, **137**, 2286–2304, https://doi.org/10.1175/2009MWR2826.1.

——, T. Sato, H. Kanamori, and F. Murata, 2017: Contrasting features of monsoon precipitation around the Meghalaya Plateau under westerly and easterly regimes. *J. Geophys. Res. Atmos.*, **122**, 9591–9610, https://doi.org/10.1002/2016JD026116.

——, ——, ——, and M. Kato, 2022: Nocturnal southerly moist surge parallel to the coastline over the western Bay of Bengal. *Geophys. Res. Lett.*, **49**, e2022GL100174, https://doi.org/10.1029/2022GL100174.

Gao, M., J. Yang, B. Wang, S. Zhou, D. Gong, and S.-J. Kim, 2018: How are heat waves over Yangtze River valley associated with atmospheric quasi-biweekly oscillation? *Climate Dyn.*, **51**, 4421–4437, https://doi.org/10.1007/s00382-017-3526-z.

Guan, P., G. Chen, W. Zeng, and Q. Liu, 2020: Corridors of mei-yu-season rainfall over eastern China. *J. Climate*, **33**, 2603–2626, https://doi.org/10.1175/JCLI-D-19-0649.1.

He, J., and B. Liu, 2016: The East Asian subtropical summer monsoon: Recent progress. *J. Meteor. Res.*, **30**, 135–155, https://doi.org/10.1007/s13351-016-5222-z.

Holton, J. R., 1967: The diurnal boundary layer wind oscillation above sloping terrain. *Tellus*, **19**, 199–205, https://doi.org/10.1111/j.2153-3490.1967.tb01473.x.

Hsu, P.-C., J.-Y. Lee, and K.-J. Ha, 2016: Influence of boreal summer intraseasonal oscillation on rainfall extremes in southern China. *Int. J. Climatol.*, **36**, 1403–1412, https://doi.org/10.1002/joc.4433.

——, ——, ——, and C.-H. Tsou, 2017: Influences of boreal summer intraseasonal oscillation on heat waves in monsoon Asia. *J. Climate*, **30**, 7191–7211, https://doi.org/10.1175/JCLI-D-16-0505.1.

Huang, S.-H., Z.-P. Wen, X.-D. Chen, Y.-Y. Guo, and Z.-W. Wang, 2022: The Henan extreme rainfall in July 2021: Modulation of the northward-shift monsoon trough on the synoptic-

scale wave train. *Adv. Climate Change Res.*, **13**, 819–825, https://doi.org/10.1016/j.accre.2022.11.001.

Huang, W.-R., J. C. L. Chan, and S.-Y. Wang, 2010: A planetary-scale land-sea breeze circulation in East Asia and the western North Pacific. *Quart. J. Roy. Meteor. Soc.*, **136**, 1543–1553, https://doi.org/10.1002/qj.663.

——, P.-Y. Liu, J.-H. Chen, and L. Deng, 2019: Impact of boreal summer intra-seasonal oscillations on the heavy rainfall events in Taiwan during the 2017 Meiyu season. *Atmosphere*, **10**, 205, https://doi.org/10.3390/atmos10040205.

Huffman, G. J., and Coauthors, 2007: The TRMM Multisatellite Precipitation Analysis (TMPA): Quasi-global, multiyear, combined-sensor precipitation estimates at fine scales. *J. Hydrometeor.*, **8**, 38–55, https://doi.org/10.1175/JHM560.1.

Ko, K.-C., and H.-H. Hsu, 2006: Sub-monthly circulation features associated with tropical cyclone tracks over the East Asian monsoon area during July-August season. *J. Meteor. Soc. Japan*, **84**, 871–889, https://doi.org/10.2151/jmsj.84.871.

Kobayashi, S., and Coauthors, 2015: The JRA-55 reanalysis: General specifications and basic characteristics. *J. Meteor. Soc. Japan*, **93**, 5–48, https://doi.org/10.2151/jmsj.2015-001.

Koo, M.-S., S.-Y. Hong, and J. Kim, 2009: An evaluation of the Tropical Rainfall Measuring Mission (TRMM) Multi-satellite Precipitation Analysis (TMPA) data over South Korea. *Asia-Pac. J. Atmos. Sci.*, **45**, 265–282.

Krishnamurti, T. N., and C. M. Kishtawal, 2000: A pronounced continental-scale diurnal mode of the Asian summer monsoon. *Mon. Wea. Rev.*, **128**, 462–473, https://doi.org/10.1175/1520-0493(2000)128<0462:APCSDM>2.0.CO;2.

Kudo, T., R. Kawamura, H. Hirata, K. Ichiyanagi, M. Tanoue, and K. Yoshimura, 2014: Large-scale vapor transport of remotely evaporated seawater by a Rossby wave response to typhoon forcing during the Baiu/Meiyu season as revealed by the JRA-55 reanalysis. *J. Geophys. Res. Atmos.*, **119**, 8825–8838, https://doi.org/10.1002/2014JD021999.

Lau, K.-M., G. J. Yang, and S. H. Shen, 1988: Seasonal and intraseasonal climatology of summer monsoon rainfall over East Asia. *Mon. Wea. Rev.*, **116**, 18–37, https://doi.org/10.1175/1520-0493(1988)116<0018:SAICOS>2.0.CO;2.

Lee, S.-S., J.-Y. Moon, B. Wang, and H.-J. Kim, 2017: Subseasonal prediction of extreme precipitation over Asia: Boreal summer intraseasonal oscillation perspective. *J. Climate*, **30**, 2849–2865, https://doi.org/10.1175/JCLI-D-16-0206.1.

Li, P., C. Moseley, A. F. Prein, H. Chen, J. Li, K. Furtado, and T. Zhou, 2020: Mesoscale convective system precipitation characteristics over East Asia. Part I: Regional differences and seasonal variations. *J. Climate*, **33**, 9271–9286, https://doi.org/10.1175/JCLI-D-20-0072.1.

Li, R. C. Y., and W. Zhou, 2015: Multiscale control of summertime persistent heavy precipitation events over South China in association with synoptic, intraseasonal, and low-frequency background. *Climate Dyn.*, **45**, 1043–1057, https://doi.org/10.1007/s00382-014-2347-6.

Li, T., and B. Wang, 2005: A review on the western North Pacific monsoon: Synoptic-to-interannual variabilities. *Terr. Atmos. Ocean. Sci.*, **16**, 285–314, https://doi.org/10.3319/TAO.2005.16.2.285(A).

Ling, Z., Y. Wang, and G. Wang, 2016: Impact of intraseasonal oscillations on the activity of tropical cyclones in summer over the South China Sea. Part I: Local tropical cyclones. *J. Climate*, **29**, 855–868, https://doi.org/10.1175/JCLI-D-15-0617.1.

Liu, B., G. Chen, W. Zeng, L. Bai, and H. Qin, 2022: Diurnal variations of southerly monsoon surge and their impacts on East Asian summer rainfall. *J. Climate*, **35**, 159–177, https://doi.org/10.1175/JCLI-D-21-0372.1.

Liu, H. B., J. Yang, D.-L. Zhang, and B. Wang, 2014: Roles of synoptic to quasi-biweekly disturbances in generating the summer 2003 heavy rainfall in East China. *Mon. Wea. Rev.*, **142**, 886–904, https://doi.org/10.1175/MWR-D-13-00055.1.

Luo, Y., and Y. Du, 2022: The roles of low-level jets in "21·7" Henan extremely persistent heavy rainfall event. *Adv. Atmos. Sci.*, **40**, 350–373, https://doi.org/10.1007/s00376-022-2026-1.

——, H. Wang, R. Zhang, W. Qian, and Z. Luo, 2013: Comparison of rainfall characteristics and convective properties of monsoon precipitation systems over South China and the Yangtze and Huai River Basin. *J. Climate*, **26**, 110–132, https://doi.org/10.1175/JCLI-D-12-00100.1.

Moncrieff, M. W., M. A. Shapiro, J. M. Slingo, and F. Molteni, 2007: Collaborative research at the intersection of weather and climate. *WMO Bull.*, **56**, 204–211, https://public-old.wmo.int/en/bulletin/collaborative-research-intersection-weather-and-climate.

Natoli, M. B., and E. D. Maloney, 2019: Intraseasonal variability of the diurnal cycle of precipitation in the Philippines. *J. Atmos. Sci.*, **76**, 3633–3654, https://doi.org/10.1175/JAS-D-19-0152.1.

Ninomiya, K., and Y. Shibagaki, 2007: Multi-scale features of the Meiyu-Baiu front and associated precipitation systems. *J. Meteor. Soc. Japan*, **85B**, 103–122, https://doi.org/10.2151/jmsj.85B.103.

Pan, H., and G. Chen, 2019: Diurnal variations of precipitation over North China regulated by the mountain-plains solenoid and boundary-layer inertial oscillation. *Adv. Atmos. Sci.*, **36**, 863–884, https://doi.org/10.1007/s00376-019-8238-3.

Qian, W., H.-S. Kang, and D.-K. Lee, 2002: Distribution of seasonal rainfall in the East Asian monsoon region. *Theor. Appl. Climatol.*, **73**, 151–168, https://doi.org/10.1007/s00704-002-0679-3.

Ren, H.-L., and Coauthors, 2023: Seamless prediction in China: A review. *Adv. Atmos. Sci.*, **40**, 1501–1520, https://doi.org/10.1007/s00376-023-2335-z.

Shen, Y., A. Xiong, Y. Wang, and P. Xie, 2010: Performance of high-resolution satellite precipitation products over China. *J. Geophys. Res.*, **115**, D02114, https://doi.org/10.1029/2009JD012097.

Shin, U., T.-Y. Lee, and S.-H. Park, 2019: Environment and processes for heavy rainfall in the early morning over the Korean peninsula during episodes of cloud clusters associated with mesoscale troughs. *J. Meteor. Soc. Japan*, **97**, 633–655, https://doi.org/10.2151/jmsj.2019-036.

Song, Z., C. Zhu, J. Su, and B. Liu, 2016: Coupling modes of climatological intraseasonal oscillation in the East Asian summer monsoon. *J. Climate*, **29**, 6363–6382, https://doi.org/10.1175/JCLI-D-15-0794.1.

Sun, J., and F. Zhang, 2012: Impacts of mountain–plains solenoid on diurnal variations of rainfalls along the mei-yu front over the East China plains. *Mon. Wea. Rev.*, **140**, 379–397, https://doi.org/10.1175/MWR-D-11-00041.1.

Sun, X., G. Jiang, X. Ren, and X.-Q. Yang, 2016: Role of intraseasonal oscillation in the persistent extreme precipitation over the Yangtze River basin during June 1998. *J. Geophys. Res. Atmos.*, **121**, 10 453–10 469, https://doi.org/10.1002/2016JD025077.

Tamaki, Y., M. Inatsu, D. Nguyen-Le, and T. J. Yamada, 2018: Heavy rainfall duration bias in dynamical downscaling and its related synoptic patterns in summertime Asian monsoon. *J.*

Appl. Meteor. Climatol., **57**, 1477–1496, https://doi.org/10.1175/JAMC-D-17-0116.1.

Wang, B., and LinHo, 2002: Rainy season of the Asian–Pacific summer monsoon. *J. Climate*, **15**, 386–398, https://doi.org/10.1175/1520-0442(2002)015<0386:RSOTAP>2.0.CO;2.

Wang, D., Y. Zhang, and A. Huang, 2013: Climatic features of the South-westerly low-level jet over southeast China and its association with precipitation over East China. *Asia-Pac. J. Atmos. Sci.*, **49**, 259–270, https://doi.org/10.1007/s13143-013-0025-y.

Wang, H., F. Liu, B. Wang, G. Chen, and W. Dong, 2021: Diversity of intraseasonal oscillation over the western North Pacific. *Climate Dyn.*, **57**, 1881–1893, https://doi.org/10.1007/s00382-021-05780-2.

Wang, L., J. Jiang, T. Li, X. Zhou, and Z. Chen, 2023: Three distinct circulation patterns that induce enhanced intraseasonal precipitation events over South China in boreal winter. *Climate Dyn.*, **60**, 2893–2905, https://doi.org/10.1007/s00382-022-06478-9.

Wei, Y., H.-L. Ren, B. Xiang, Y. Wang, J. Wu, and S. Wang, 2023: Diverse MJO genesis and predictability. *Bull. Amer. Meteor. Soc.*, **104**, E792–E809, https://doi.org/10.1175/BAMS-D-22-0101.1.

Wu, G., and Coauthors, 2007: The influence of mechanical and thermal forcing by the Tibetan Plateau on Asian climate. *J. Hydrometeor.*, **8**, 770–789, https://doi.org/10.1175/JHM609.1.

Wu, R., G. Chen, and Z. J. Luo, 2023: Strong coupling in diurnal variations of clouds, radiation, winds, and precipitation during the East Asian summer monsoon. *J. Climate*, **36**, 1347–1368, https://doi.org/10.1175/JCLI-D-22-0330.1.

Xu, J., R. Li, Q. Zhang, Y. Chen, X. Liang, and X. Gu, 2022: Extreme large-scale atmospheric circulation associated with the "21·7" Henan flood. *Sci. China Earth Sci.*, **65**, 1847–1860, https://doi.org/10.1007/s11430-022-9975-0.

Xu, W., E. J. Zipser, and C. Liu, 2009: Rainfall characteristics and convective properties of mei-yu precipitation systems over South China, Taiwan, and the South China Sea. Part I: TRMM observations. *Mon. Wea. Rev.*, **137**, 4261–4275, https://doi.org/10.1175/2009MWR2982.1.

——, S. A. Rutledge, and K. Chudler, 2021: Diurnal cycle of coastal convection in the South China Sea region and modulation by the BSISO. *J. Climate*, **34**, 4297–4314, https://doi.org/10.1175/JCLI-D-20-0308.1.

Xue, M., X. Luo, K. Zhu, Z. Sun, and J. Fei, 2018: The controlling role of boundary layer inertial oscillations in Meiyu frontal precipitation and its diurnal cycles over China. *J. Geophys. Res. Atmos.*, **123**, 5090–5115, https://doi.org/10.1029/2018JD028368.

Yang, H., and C. Li, 2003: The relation between atmospheric intraseasonal oscillation and summer severe flood and drought in the Changjiang–Huaihe River basin. *Adv. Atmos. Sci.*, **20**, 540–553, https://doi.org/10.1007/BF02915497.

Yang, J., B. Wang, and Q. Bao, 2010: Biweekly and 21–30-day variations of the subtropical summer monsoon rainfall over the lower reach of the Yangtze River basin. *J. Climate*, **23**, 1146–1159, https://doi.org/10.1175/2009JCLI3005.1.

——, Q. Bao, B. Wang, D.-Y. Gong, H. He, and M.-N. Gao, 2014: Distinct quasi-biweekly features of the subtropical East Asian monsoon during early and late summers. *Climate Dyn.*, **42**, 1469–1486, https://doi.org/10.1007/s00382-013-1728-6.

Yang, Y.-M., J.-Y. Lee, and B. Wang, 2020: Dominant process for northward propagation of boreal summer intraseasonal oscillation over the western North Pacific. *Geophys. Res. Lett.*, **47**, e2020GL089808, https://doi.org/10.1029/2020GL089808.

Yu, R., J. Li, and H. Chen, 2009: Diurnal variation of surface wind over central eastern China. *Climate Dyn.*, **33**, 1089–1097, https://doi.org/10.1007/s00382-008-0478-3.

Yuan, W., R. Yu, M. Zhang, W. Lin, J. Li, and Y. Fu, 2013: Diurnal cycle of summer precipitation over subtropical East Asia in CAM5. *J. Climate*, **26**, 3159–3172, https://doi.org/10.1175/JCLI-D-12-00119.1.

Zeng, W., G. Chen, L. Bai, Q. Liu, and Z. Wen, 2022: Multiscale processes of heavy rainfall over East Asia in summer 2020: Diurnal cycle in response to synoptic disturbances. *Mon. Wea. Rev.*, **150**, 1355–1376, https://doi.org/10.1175/MWR-D-21-0308.1.

Zhang, S.-L., S.-Y. Tao, Q.-Y. Zhang, and J. Wei, 2002: Large and meso-α scale characteristics of intense rainfall in the mid- and lower reaches of the Yangtze River. *Chin. Sci. Bull.*, **47**, 779–786, https://doi.org/10.1360/02tb9176.

Zhang, Y., F. Zhang, C. A. Davis, and J. Sun, 2018: Diurnal evolution and structure of long-lived mesoscale convective vortices along the mei-yu front over the East China plains. *J. Atmos. Sci.*, **75**, 1005–1025, https://doi.org/10.1175/JAS-D-17-0197.1.

——, M. Xue, K. Zhu, and B. Zhou, 2019: What is the main cause of diurnal variation and nocturnal peak of summer precipitation in Sichuan Basin, China? The key role of boundary layer low-level jet inertial oscillations. *J. Geophys. Res. Atmos.*, **124**, 2643–2664, https://doi.org/10.1029/2018JD029834.

Zhao, R., K. Wang, G. Wu, and C. Zhou, 2021: Temperature annual cycle variations and responses to surface solar radiation in China between 1960 and 2016. *Int. J. Climatol.*, **41**, E2959–E2978, https://doi.org/10.1002/joc.6895.

Zhao, T., and A. Yatagai, 2014: Evaluation of TRMM 3B42 product using a new gauge-based analysis of daily precipitation over China. *Int. J. Climatol.*, **34**, 2749–2762, https://doi.org/10.1002/joc.3872.

Zheng, B., and Y. Huang, 2019: Mechanisms of northward-propagating intraseasonal oscillation over the South China Sea during the pre-monsoon period. *J. Climate*, **32**, 3297–3311, https://doi.org/10.1175/JCLI-D-18-0391.1.

Zhou, T., R. Yu, H. Chen, A. Dai, and Y. Pan, 2008: Summer precipitation frequency, intensity, and diurnal cycle over China: A comparison of satellite data with rain gauge observations. *J. Climate*, **21**, 3997–4010, https://doi.org/10.1175/2008JCLI2028.1.